photonics

MDPI

Review

Fourier Transform Holography: A Lensless Imaging Technique, Its Principles and Applications

Sara Mustafi [1,2] and Tatiana Latychevskaia [1,2,*]

[1] Paul Scherrer Institute, CH-5232 Villigen, Switzerland
[2] Department of Physics, University of Zurich, CH-8057 Zurich, Switzerland
* Correspondence: tatiana@physik.uzh.ch; Tel.: +41-56-310-4679

Abstract: Fourier transform holography (FTH) is a lensless imaging technique where the wave scattered by an object is superimposed with the wave scattered by a reference source positioned in the same plane. The distribution of the object is then reconstructed by simply calculating the Fourier transform of the recorded hologram. In this study, we outline the basic principles of FTH and provide an overview of the different types of references and the associated reconstruction algorithms. Current applications of FTH with different waves (light, electron, and X-ray) are presented, and their relationships with other coherent imaging techniques are discussed.

Keywords: holography; Fourier transform holography; phase problem; coherent diffraction imaging

1. Introduction

1.1. Phase Problem

Holography was proposed as a lensless imaging technique by Dennis Gabor in 1947 in an attempt to solve the problem of limited resolution in electron microscopes due to lens aberrations [1–3]. Holography is an elegant solution to the so-called phase problem, which exists in coherent imaging and can be described as follows. A probing wave propagates through a sample and reaches a distant detector. Since detectors can only record intensity, information about the phase distribution of the wave is lost. However, this missing phase distribution is crucial because it contains information about the scattering events that have taken place inside the sample. Therefore, in order to reconstruct the sample distribution, the phases missing in the detector plane must be recovered. This constitutes the phase problem. Holography solves the phase problem by adding a reference wave with a known distribution to the unknown object wave. The contrast of the resulting interference pattern (the hologram) is proportional to the difference between the phases of the object and the reference waves. Thus, by knowing the phase distribution of the reference wave, it is possible for the phase distribution of the object wave, and subsequently the object distribution, to be reconstructed from the hologram.

Another example of a solution to the phase problem is coherent diffraction imaging (CDI). CDI is a high-resolution imaging technique that is similar to a diffraction experiment on crystals but involves imaging a single, isolated object rather than a crystal. In CDI, diffracted (or scattered) waves are recorded in the far field. The resulting diffraction pattern is invariant to the lateral shifts of the sample, which allows for the preservation of high-order diffraction signal. The missing phases are typically recovered by applying numerical iterative methods [4–9]. The following requirements must be met in a CDI experiment: the object under study must be isolated, and the size of the reconstructed field of view must exceed the size of the object at least twice in each direction (the oversampling condition) [9]. CDI offers the possibility of recording high-resolution information, and the associated resolution is only limited by the size of the detector.

Citation: Mustafi, S.; Latychevskaia, T. Fourier Transform Holography: A Lensless Imaging Technique, Its Principles and Applications. *Photonics* **2023**, *10*, 153. https://doi.org/10.3390/photonics10020153

Received: 11 December 2022
Revised: 24 January 2023
Accepted: 27 January 2023
Published: 1 February 2023

1.2. Fourier Transform Holography (FTH)

Since the invention of holography, its principle has found numerous applications and can be summarised as follows: any complex-valued object signal can be stored as an intensity distribution by adding a known reference signal and recording the intensity of the resulting interference pattern. In conventional holography, a reference wave is added to a complex-valued object wave in real space. In Fourier transform holography (FTH), a reference wave is added to the complex-valued spectrum of an object wave in Fourier space. Both approaches allow the complete distribution of a complex-valued object signal to be captured.

The principle of FTH was first outlined by Winthrop and Worthington in 1965 [10] as a solution to the phase problem in X-ray imaging. In the same year, Stroke demonstrated the first FTH experiment using laser light [11]. In the simplest form of FTH, a reference wave is created in Fourier space as a wave originating from a point-like source in real space, the object and point-like reference are positioned in the same plane [10–12]. The wave diffracted by the object interferes with the reference wave in the far field, and the resulting interference pattern forms the Fourier transform (FT) hologram. The FTH combines the key advantages of two other lensless imaging techniques: holography [2,3] and coherent diffraction imaging (CDI) [5]. In a similar way to holography, the added reference wave solves the phase problem. In a similar way to CDI, the scattered (or diffracted) waves are recorded in the far field, which allows for the acquisition of high-resolution information. The advantage of FTH is that reconstruction can be obtained in one step, by calculating the FT of the recorded hologram.

This paper is organised as follows. In the second section, the basic principles of FTH are outlined. In the third section, typical experimental arrangements and references for FTH are overviewed and compared. In the fourth section, a review of FTH performed with different waves (light, electron, and X-ray) is provided. In the fifth section, an overview of FTH applications is presented. In the sixth section, relationships between FTH and other coherent imaging techniques are considered. In the last section, the current challenges and perspectives of using FTH are discussed.

2. Principles of FTH

Holography is an interferometry-based technique. An object distribution is not imaged directly but reconstructed from an interference pattern formed by the superposition of the wave scattered by the object and a reference wave. In FTH, the reference wave is created by the diffraction on a reference feature (named as "reference" further in the text) which is added to the same plane as that of the studied object. Throughout this text, we will refer to the arrangement of the object and the reference altogether as the "sample." The typical scheme for recording an FT hologram is shown in Figure 1a. FTH has two distinct features: (1) an FT hologram is acquired in the far field, and (2) a reference wave is formed by the diffraction on a reference which is positioned in the same plane as the object under study (Figure 1b). The presence of the reference wave ensures that the phase distribution of the wave diffracted by an unknown object wave is captured, which solves the phase problem and simplifies the reconstruction procedure. The reference wave should cover the entire detector area, as illustrated in Figure 1c,d. In the simplest form of FTH, which uses a single point-like reference, the object reconstruction is obtained in one step, by calculating the FT of the recorded hologram, as shown in Figure 1e and explained in the next sub-sections.

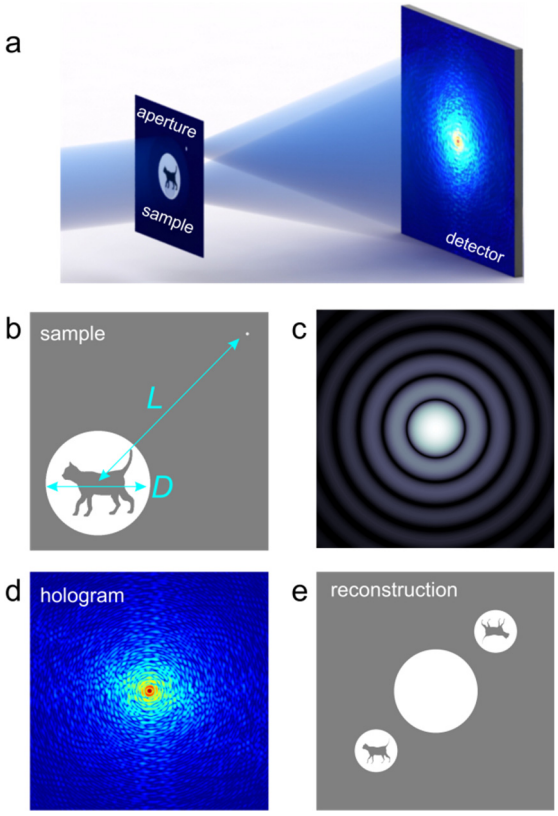

Figure 1. Principle of Fourier transform holography (FTH) with point-like reference. (**a**) Scheme for Fourier hologram acquisition. (**b**) Sample distribution: object and reference aperture. D is the extent (diameter) of the object, and L is the distance between the object and the reference. (**c**) Diffraction pattern of the reference alone. (**d**) Diffraction pattern of the object and the reference together—Fourier transform hologram. (**e**) Sample distribution (amplitude) reconstructed by calculating the Fourier transform of the Fourier transform hologram, exhibiting two centro-symmetric reconstructions at the reference position.

2.1. Hologram Formation

When the sample is illuminated by a plane wave, the wave behind the sample (the exit wave) is given by the transmission function of the sample: $u(x,y) = t(x,y)$. In an FTH arrangement, the exit wave can be represented as a sum of two terms:

$$u(x,y) = u_o(x,y) + u_r(x,y), \tag{1}$$

where $u_o(x,y)$ is the object wave term, $u_r(x,y)$ is the reference wave term, and $\vec{r} = (x,y)$ is the coordinate in the sample plane. The diffracted wavefront in the far field is given by the Huygens–Fresnel integral transform:

$$U(\vec{R}) = -\frac{i}{\lambda}\iint u(\vec{r})\frac{\exp\left(ik\left|\vec{r}-\vec{R}\right|\right)}{\left|\vec{r}-\vec{R}\right|}\mathrm{d}\sigma, \tag{2}$$

where $\vec{R} = (X,Y,Z)$ is the coordinate in the far field, k is the wavenumber $k = \frac{2\pi}{\lambda}$, λ is the wavelength, and the integration is performed over the sample plane. The integration in all integrals in this manuscript is performed over a finite area in the sample (or detector) plane.

Equation (2) can be written in Cartesian coordinates. Using the Taylor series expansion:

$$\left|\vec{r}-\vec{R}\right| \approx Z+\frac{(X-x)^2+(Y-y)^2}{2Z},$$

Equation (2) can be re-written as:

$$U(X,Y) \approx -\frac{i}{\lambda Z}\exp\left(\frac{2\pi i}{\lambda}Z\right)\exp\left[\frac{2\pi i}{\lambda Z}\left(X^2+Y^2\right)\right]\iint u(x,y)\exp\left[-\frac{2\pi i}{\lambda Z}(xX+yY)\right]\mathrm{d}x\mathrm{d}y,$$

and the hologram intensity distribution is given by:

$$I_{\mathrm{H}}(X,Y) \propto \left|\iint u(x,y)\exp\left[-\frac{2\pi i}{\lambda Z}(xX+yY)\right]\mathrm{d}x\mathrm{d}y\right|^2 = |\mathrm{FT}[u(x,y)]|^2. \quad (3)$$

Equation (2) can be written in Fourier or *K*-coordinates, as:

$$U(\vec{R}) = -\frac{i}{\lambda}\int u(\vec{r})\frac{\exp\left(ik\left|\vec{r}-\vec{R}\right|\right)}{\left|\vec{r}-\vec{R}\right|}\mathrm{d}\vec{r} \approx -\frac{i}{\lambda R}\int u(\vec{r})\exp(ikR)\exp\left(-i\vec{K}\vec{r}\right)\mathrm{d}\vec{r},$$

where the following approximation was used: $\left|\vec{r}-\vec{R}\right| \approx R-\frac{\vec{r}\vec{R}}{R}$, and $\vec{K}$ was introduced as:

$$\vec{K} = k\frac{\vec{R}}{R} = \frac{2\pi}{\lambda}\left(\frac{X}{R},\frac{Y}{R},\frac{Z}{R}\right)$$

where $R=\sqrt{X^2+Y^2+Z^2}$. At $Z^2 \gg X^2+Y^2$ the vector components can be approximated as $\vec{K} \approx \frac{2\pi}{\lambda}\left(\frac{X}{Z},\frac{Y}{Z},1\right)$. This gives:

$$U(K_x,K_y) \approx -\frac{i}{\lambda R}\exp(ikR)\int u(x,y)\exp\left[-i\left(xK_x+yK_y\right)\right]\mathrm{d}x\mathrm{d}y$$

and:

$$I_{\mathrm{H}}(K_x,K_y) \propto \left|\iint u(x,y)\exp\left[-i\left(xK_x+yK_y\right)\right]\mathrm{d}x\mathrm{d}y\right|^2 = |\mathrm{FT}[u(x,y)]|^2. \quad (4)$$

Thus, in Cartesian or Fourier coordinates, the intensity distribution in the far field is given by the squared amplitude of the FT of the exit wave. Cartesian coordinates are conventionally used in light-optical experiments, whereas Fourier domain coordinates are typically used in X-ray imaging.

2.2. Reconstruction of the Sample Distribution from the Hologram

The object distribution can be reconstructed from its FT hologram by simply calculating the inverse FT (IFT) or FT of the hologram. This can be explained as follows. The autocorrelation of $u(x,y)$ by definition is given by:

$$u(x,y)\circ u(x,y) = \iint u^*(\mu,\eta)\,u(\mu+x,\eta+y)\mathrm{d}\mu\mathrm{d}\eta, \quad (5)$$

where $\circ$ denotes correlation. The FT of the autocorrelation is calculated as:

$$\mathrm{FT}[u(x,y)\circ u(x,y)] = \iint\iint u^*(\mu,\eta)\,u(\mu+x,\eta+y)\exp[-2\pi i(xv+yw)]\mathrm{d}\mu\mathrm{d}\eta\mathrm{d}x\mathrm{d}y, \quad (6)$$

which can be re-written in thenew coordinates, $\mu + x = x'$ and $\eta + y = y'$, or $x = x' - \mu$ and $y = y' - \eta$, as:

$$\begin{aligned} &\mathrm{FT}[u(x,y) \circ u(x,y)] = \\ &\iint u^*(\mu,\eta)\ \exp[2\pi i(\mu v + \eta w)]\mathrm{d}\mu\mathrm{d}\eta \iint u(x',y')\ \exp[-2\pi i(x'v + y'w)]\mathrm{d}x'\mathrm{d}y' = \\ &\{\mathrm{FT}[u(x,y)]\}^*\mathrm{FT}[u(x,y)] = |\mathrm{FT}[u(x,y)]|^2 = I_\mathrm{H}, \end{aligned} \tag{7}$$

where we used the expressions given by Equations (3) or (4). A similar result is known from signal theory: the Wiener–Chintchin theorem states that the FT of a signal's autocorrelation function gives the signal's spectral power [13,14].

From Equation (7), it follows that the IFT of the intensity distribution (hologram) gives the autocorrelation of the exit wave:

$$\mathrm{IFT}(I_\mathrm{H}) = \iint u^*(\mu,\eta)\ u(\mu + x, \eta + y)\mathrm{d}\mu\mathrm{d}\eta = u(x,y) \circ u(x,y). \tag{8}$$

In the simplest form of FTH, the reference $u_r(x,y)$ is a tiny hole or a point-like scatterer, which can be mathematically described as a δ-function. The exit wave behind the sample can be written as:

$$u(x,y) = u_o(x,y) + \delta(x - x_0, y - y_0), \tag{9}$$

where (x_0, y_0) is the position of the point-like reference. The IFT of the FT hologram gives the autocorrelation of the exit wave (or transmission function):

$$u(x,y) \circ u(x,y) = \delta(x,y) + u_o(x,y) \circ u_o(x,y) + u_o(x + x_0, y + y_0) + {u_o}^*(-x + x_0, -y + y_0). \tag{10}$$

Here, the first term describes a sharp intensity peak at the centre. The second term describes the autocorrelation of the object distribution, which is also located in the centre and is about twice the size of the object. The third term describes the object distribution centred at the $(-x_0, -y_0)$ coordinate. The fourth term describes the complex-conjugated centro-symmetrically flipped object distribution centred at the (x_0, y_0) coordinate, as shown in Figure 1e. When FT is used instead of IFT, the reconstructed distribution is centro-symmetrically flipped: $u(-x,-y) \circ u(-x,-y) \propto u_o(-x + x_0, -y + y_0) + {u_o}^*(x + x_0, y + y_0)$. Here, the third term describes the centro-symmetrically flipped reconstructed object distribution at the (x_0, y_0) coordinate, and the fourth term describes the reconstructed complex-conjugated object distribution at the $(-x_0, -y_0)$ coordinate. Thus, in principle, the object distribution can be reconstructed by calculating either the FT or IFT of its FT hologram.

In the simplest form of FTH with a single point-like reference, a single Fourier transform (FT or IFT) of the hologram is sufficient to obtain the reconstruction. More complicated references and the related reconstruction algorithms are discussed below.

2.3. Optimal Parameters

2.3.1. Distance between the Object and the Reference

The optimal distance between the object and the reference follows from Equation (10). To avoid an overlap of the reconstructed-object and object autocorrelation distributions, the object and reference must be separated by a distance L that should be at least 1.5 times larger than the extent of the object D (Figure 1b):

$$L > 1.5D. \tag{11}$$

Most FTH arrangements follow this rule. Even for FTH, where the object reconstruction is obtained using iterative methods, the initial reconstruction obtained by a single IFT should exhibit the object and the centred autocorrelation distributions as being spatially separated, which is achieved by setting the parameters according to Equation (11).

2.3.2. The Reconstructed Field of View

The reconstructed field of view must be large enough to include all the reconstructed distributions (the object's autocorrelation and the two sidebands as shown in Figure 1e). This is achieved by setting the parameters of the experimental setup as follows. The relationship between the diffraction pattern parameters and the reconstructed field of view follows from the expression for IFT that is employed for reconstruction:

$$u_{\mathrm{rec}}(x,y) = \iint I_{\mathrm{H}}(X,Y) \exp\left[\frac{2\pi i}{\lambda Z}(Xx+Yy)\right] \mathrm{d}X\mathrm{d}Y \tag{12}$$

which in digital form is expressed via fast FT (FFT) as:

$$u_{\mathrm{rec}}(m,n) = \sum_{p,q=0}^{N-1} I_{\mathrm{H}}(p,q) \exp\left[\frac{2\pi i}{N}(pm+qn)\right] \tag{13}$$

where the coordinates (x,y) are digitised as $x \to \Delta_x m, y \to \Delta_y n$, the coordinates (X,Y) are digitised as $X \to \Delta_X p, Y \to \Delta_Y q$, $\Delta_x = \Delta_y$ is the pixel size in the sample plane, $\Delta_X = \Delta_Y$ is the pixel size in the detector plane, and $m,n,p,q = 0 \ldots N-1$ are the pixel numbers. Through comparing Equations (12) and (13), one obtains the condition:

$$\frac{1}{\lambda Z}\Delta_X \Delta_x = \frac{1}{N} \tag{14}$$

and the reconstructed field of view:

$$s_0 = N\Delta_x = \frac{\lambda Z}{\Delta_X}. \tag{15}$$

The reconstructed field of view should be large enough to entail the four distributions reconstructed from an FT hologram, and, therefore, must be larger than $s_0 > 4D$. This leads to the following relationship between the parameters of a setup for FTH:

$$\frac{\lambda Z}{\Delta_X} > 4D. \tag{16}$$

In K-coordinates, the expression for IFT that is employed for reconstruction is given by:

$$u_{\mathrm{rec}}(x,y) = \iint I_{\mathrm{H}}(K_x,K_y) \exp\left[i(K_x x + K_y y)\right] \mathrm{d}K_x \mathrm{d}K_y, \tag{17}$$

where the FFT given by Equation (13) leads to the following equation:

$$\Delta_K \Delta_x = \frac{2\pi}{N}, \tag{18}$$

which gives the reconstructed field of view:

$$s_0 = N\Delta_x = \frac{2\pi}{\Delta_K} \tag{19}$$

and the relationship between the parameters of a setup for FTH:

$$\frac{2\pi}{\Delta_K} > 4D. \tag{20}$$

2.3.3. The Detector Parameters

The size of the detector determines the numerical aperture of the setup and therefore defines the theoretical limit of the resolution of the reconstructed object distribution as $R = \lambda/2\mathrm{NA}$, where NA is the numerical aperture of the setup. The same resolution can also be obtained as the pixel size in the sample plane from Equation (14): $\Delta_x = \frac{\lambda Z}{N\Delta_X} = \frac{\lambda Z}{S}$ for Cartesian coordinates and from Equation (18): $\Delta_x = \frac{2\pi}{N\Delta_K}$ for K-coordinates. Here, the "detector size", given by $S \times S$, is not the physical size of the detector but its effective size, that is, the area where hologram intensity is high enough to be detected.

The detector's pixel size provides the extent of the reconstructed field of view in the sample plane, as given by Equations (15) and (19) for Cartesian coordinates and K-coordinates, respectively.

Like diffraction patterns, FT holograms exhibit a large range of intensity values with high intensity values in their centres and lower intensity values towards their edges. Moreover, the signal at the edges of an FT hologram defines the resolution of the reconstructed object. In order to accurately capture all the intensity values from the centre to the edges of an FT hologram, detectors with high dynamic range (16 bits or higher) are preferred [9]. Low-cost cameras can also be employed by acquiring a set of images at different exposures and then recombining them into one high-dynamic-range image, as demonstrated in [15,16].

2.3.4. Reference Size and Resolution

The size of the reference defines the resolution of the reconstructed object and therefore should be sufficiently small. Shortly after the invention of FTH, the effect of reference size was studied, and it was shown that resolution was inversely proportional to reference size [17]. On the other hand, the size of the reference should be sufficiently large to ensure that the object and reference waves exhibit comparable intensity values. The size of the reference is scaled with the wavelength. Some values of references sizes are provided in the sections where specific reference types are discussed in detail. In addition, the shape of the reference also plays a role. The zeros in the Fourier spectrum of a reference lead to missing information in the FT hologram, which in turn leads to a reduced quality of the reconstructed object. Thus, finding a perfectreference in terms of size and shape is both theoretically and experimentally challenging. There is an ongoing search for optimal references, and some of the proposed and demonstrated references are discussed in the next sections.

3. Types of References

An overview of the most typical references for FTH is shown in Figure 2. The simplest reference is a point-like reference (Figure 2a). A disadvantage of using a single point-like reference is that it provides a relatively weak reference wave when compared to the object wave. To solve this problem, various references have been proposed (Figure 2b–f), which will be discussed in the following sub-sections. Some of the references (for example, single point-like reference, multiple point-like references, and an object inside a squared-aperture support) allow for easy reconstruction by applying a single IFT (or FT) to the recorded hologram. Other references (for example, extended references, uniformly redundant array (URA) references, and arbitrary references) allow the intensities of object and reference waves to be equalised but require a more complicated data analysis, as discussed in detail below. In X-ray imaging—the main field for FTH applications—the simplest form of FTH, with a single point-like reference, remains the best choice for the simplicity of both nanofabrication and data analysis.

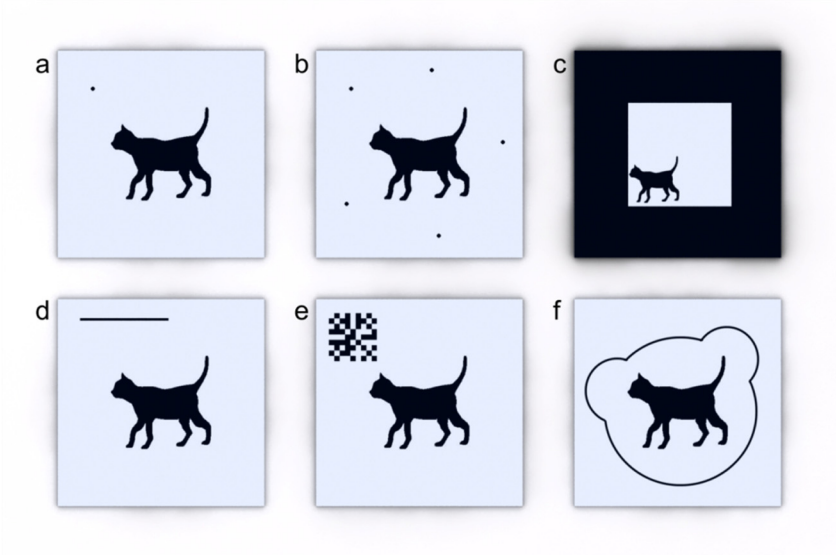

Figure 2. Overview of the different types of references for Fourier transform holography: (**a**) single point-like reference, (**b**) multiple point-like references, (**c**) object inside a squared-aperture support, (**d**) extended reference, (**e**) uniformly redundant array (URA) reference, and (**f**) arbitrary reference. The sizes and positions of the references are not to scale for purposes of presentation.

3.1. Point-like References

3.1.1. Single Point-like Reference

In the simplest form of FTH, the reference wave originates from a point-like reference, which in practice can be a small aperture or a point-like scatterer (Figure 2a). A single point-like reference allows for the easiest reconstruction procedure, which requires simply calculating the IFT of the hologram. The first experimental light-optical FTH employed a single point-like reference, as shown in Figure 3 [11,12]. In these light-optical experiments, both the object and the reference were created as apertures in an opaque material. Using a small aperture as the reference is a more typical choice. However, it was also shown that a tiny particle that was unintentionally present in the object plane could serve as a reference and produce an FT hologram [16].

Besides being used in light-optical FTH [11,12,16–19], single point-like references are also widely used in X-ray FTH [20–37]. The optimal diameter of the reference aperture is in scale with the wavelength. For light-optical FTH, the diameter of the aperture can be a few tens of microns, ranging from 10 μm [18] to 500 μm [12]. In X-ray FTH, the aperture's diameter is a few microns, for example 1.5 μm in [22] These tiny apertures are typically produced using focused-ion-beam technology.

The apertures for X-ray FTH are fabricated as holes in a thick material and therefore they exhibit a three-dimensional (3D) shape. The diffraction of plane waves from circular apertures of finite thickness was previously investigated in [38,39], where the authors reported that 3D-tube-like apertures did not exhibit a classical Airy pattern that is produced by an aperture in infinitely thin, opaque material. The effect of the 3D shape of reference apertures was recently studied by Malm et al. [37]. The authors investigated a 3D aperture with a profile consisting of a tunnel and a funnel, and they recorded the diffraction patterns in two different orientations of the aperture: one with the large (funnel) towards the illuminating beam, and the other one with the small (tunnel) opening towards the illuminating beam. The authors measured a stronger scattering at higher diffraction angles in the case when the beam entered from the funnel side (larger opening). A strong reference signal, particularly at high scattering angles, leads to a higher signal-to-noise ratio in the recorded hologram, which, in turn, results in better resolution of the reconstructed objects [37].

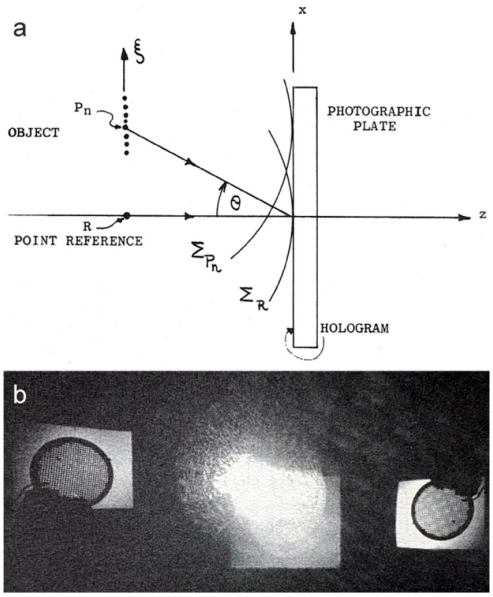

Figure 3. The first experimental realisation of Fourier transform holography (FTH) by Stroke in 1965. (**a**) Schematics of the light-optical experiment and (**b**) reconstruction of the sample. The recording and reconstruction were performed using a 632.8 Å laser light. P_n are the points of the object, θ is the incident angle, Σ_{Pn} and Σ_R are the two spherical wavefronts, z is the optical axis, and ξ and x are the axes in the object and hologram planes, respectively. Reprinted from G. W. Stroke, "Lensless Fourier-transform method for optical holography", Applied Physics Letters 6 (10), 201–203 (1965) [11], with the permission of AIP Publishing.

3.1.2. Multiple Point-like References

To increase the intensity of a reference wave, multiple point-like references can be used instead of a single point-like reference [40–73], as illustrated in Figure 2b. Each point-like reference gives rise to two reconstructed object distributions located at centro-symmetrical positions, as shown in Figure 4. When using multiple point-like references, the position of each point-like reference is selected in such a way that there is no other centro-symmetrical point-like reference (note a five-fold symmetry in the arrangement of the point-like references shown in Figure 4). Each point-like reference reconstructs the entire sample distribution, including the other point-like references, which can lead to an unwanted superposition of the reconstructed object distributions. The object reconstructed from each reference has its resolution defined by the size of that reference.

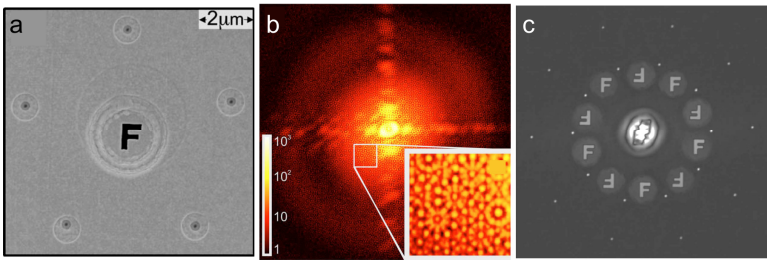

Figure 4. Fourier transform holography with multiple references. (**a**) Scanning electron micrograph (SEM) of the sample. (**b**) Diffraction pattern acquired with coherent soft X-rays (λ = 1.58 nm, E = 780 eV). Enlargement shows details of the interference pattern characteristics for the five reference sources. (**c**) The reconstruction obtained by calculating the Fourier transform of the recorded hologram shown in (**b**). Reprinted from W. F. Schlotter, R. Rick, K. Chen, A. Scherz, J. Stohr, J. Luning, S. Eisebitt, C. Gunther, W. Eberhardt, O. Hellwig, I. McNulty, "Multiple reference Fourier transform holography with soft x rays", Applied Physics Letters 89 (16), 163112 (2006) [40], with the permission of AIP Publishing.

3.2. Extended References

3.2.1. References in the Form of Geometrical Shapes

In 2007, Podorov et al. suggested placing the object into a uniformly illuminated rectangular aperture with dimensions at least two times larger than those of the object [74], as illustrated in Figures 2c and 5a–c. For this sample arrangement, the reconstruction is obtained by calculating the IFT of the product $I_{\mathrm{H}}(K_x, K_y)K_xK_y$:

$$u_{\mathrm{rec}}(x, y) = \mathrm{IFT}\left[I_{\mathrm{H}}(K_x, K_y)K_xK_y\right]. \tag{21}$$

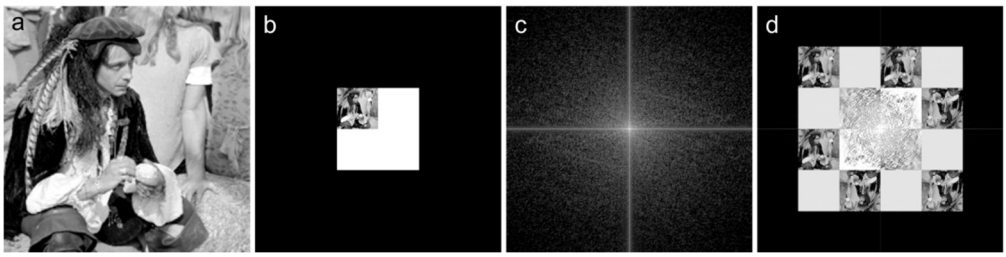

Figure 5. Fourier transform holography with an object placed inside a squared-aperture support. (**a**) Object distribution. (**b**) Distribution of the sample, where the object is placed inside a squared-aperture support that is at least twice as large as the object. (**c**) Diffraction pattern (Fourier transform hologram) of the sample shown in (**b**). (**d**) Reconstructed distribution.

The obtained reconstructed distribution exhibits eight reconstructed objects, six of which are well separated, as shown in Figure 5d. The original paper by Podorov et al. [74] provided only simulations, and a light-optical experiment was performed later that showed that the quality of the obtained reconstruction was relatively poor when compared with the reconstruction obtained from Gabor-type hologram of the same object [75], as shown in Figure 18. Podorov et al.'s idea to use a well-defined geometrical support as a reference triggered a new direction of using various geometrical shapes with sharp edges as reference.

Holography with extended reference by autocorrelation linear differential operation (HERALDO) combines all types of FTH that are realised with references in the form of geometrical shapes with sharp edges (lines, triangles, parallelograms, etc.), as shown in Figure 2d. This concept, with simulations, was proposed by Guizar-Sicairos et al. in 2007 [76] and optical experiments were performed by Guizar-Sicairos et al. in 2008 [77]. The experimental results are shown in Figure 6. The reconstruction of a HERALDO-type FT hologram requires computation of the directional derivatives of the exit-wave autocorrelation. Because this autocorrelation is calculated as the IFT of the measured hologram, the directional derivatives are calculated by computing the IFT of the product of the measured hologram and the corresponding polynomial [77]:

$$u_{\mathrm{rec}}(x, y) = \mathrm{IFT}\left[I_{\mathrm{H}}(K_x, K_y)p\left(K_x, K_y\right)\right], \tag{22}$$

where $p\left(K_x, K_y\right)$ describes a polynomial function. HERALDO has been demonstrated with visible light [77,78] and X-rays [79–89]. A combination of HERALDO and an iterative phase retrieval was demonstrated in [78].

The resolution of an object reconstructed from FT holograms with extended reference is defined by the parameters of the reference, for example, by the slit width in the case of a slit reference. Boutu et al. compared reconstructions that were obtained from FT holograms that employed round-, slit-, and square-shaped apertures as references and showed that the best quality and highest resolution reconstructed objects were obtained using a slit-aperture reference [86].

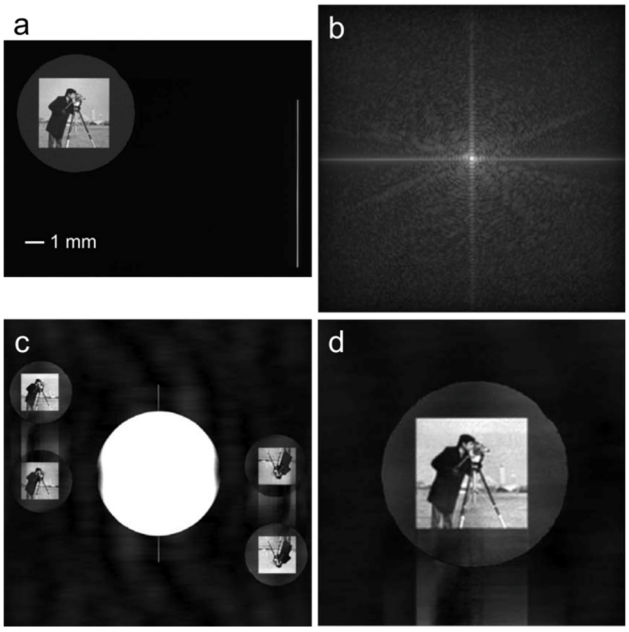

Figure 6. Holography with extended reference by autocorrelation linear differential operation (HERALDO) light-optical experimental results; photograph of the "cameraman" was printed on a slide. (**a**) Amplitude distribution of the sample: object with a thin-slit reference. (**b**) Measured intensity pattern (Fourier transform hologram). (**c**) Reconstruction obtained by calculating the inverse Fourier transform of the product $i2\pi K_y I_H(K_x, K_y)$ and (**d**) the magnified region of (**c**) showing the upper reconstruction. Adapted with permission from M. Guizar-Sicairos and J. R. Fienup, "Direct image reconstruction from a Fourier intensity pattern using HERALDO", Optics Letters 33 (22), 2668–2670 (2008) [77], © The Optical Society.

3.2.2. Uniformly Redundant Array (URA) Reference

Uniformly redundant array (URA) is a patterned optical element with flat power spectrum [90]. Using a URA as a reference in FTH (Figure 2e) allows for the preservation of all frequencies in the object spectrum, and therefore, in the reconstructed object distribution. In FTH with a URA reference [91–93], the FT of the hologram gives a central intensity distribution and two sideband distributions, the latter being a cross-correlation of the object and URA distributions, as shown in Figure 7. One sideband is selected by multiplying the entire obtained distribution with a binary mask, which sets the values outside the selected region to zero, as shown in Figure 7. The final reconstruction is then obtained by applying a delta-Hadamard transform [94] to the selected region. The initial resolution of the reconstructed object is given by the resolution of the URA, and it can be enhanced by applying iterative phase retrieval methods [95,96].

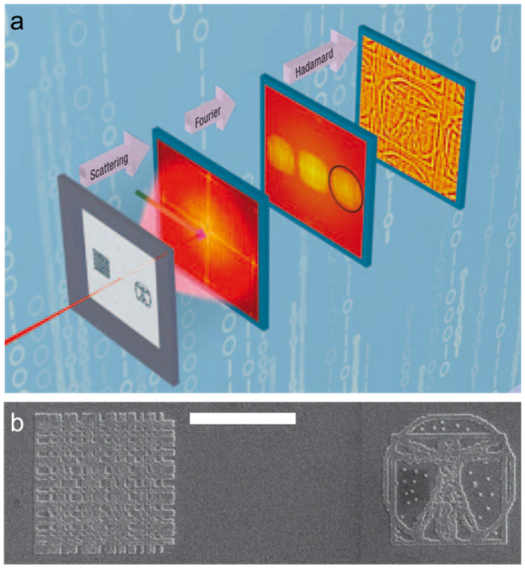

Figure 7. Fourier transform holography with uniformly redundant array (URA). (**a**) Experimental arrangement and the steps of the reconstruction procedure. (**b**) Scanning electron micrograph (SEM) of the sample, exhibiting the structure of the URA; scalebar is 2 μm. Reproduced from S. Marchesini, S. Boutet, A. E. Sakdinawat, M. J. Bogan, S. Bajt, A. Barty, H. N. Chapman, M. Frank, S. P. Hau-Riege, A. Szoke, C. W. Cui, D. A. Shapiro, M. R. Howells, J. C. H. Spence, J. W. Shaevitz, J. Y. Lee, J. Hajdu, M. M. Seibert, "Massively parallel X-ray holography", Nature Photonics 2 (9), 560–563 (2008) [91], with permission from Springer Nature.

3.2.3. Arbitrary Extended Reference

3.2.3.1. Reconstruction by Deconvolution

FTH can be realised with an arbitrarily shaped extended reference (Figure 2f). According to Equations (3) and (4), the hologram intensity distribution contains the FT of the object wave: $I_{\mathrm{H}} = |\mathrm{FT}(u)|^2 = |\mathrm{FT}(u_r + u_o)|^2 = |U_r + U_0|^2 \propto U_r^* U_0$, where $U_r = \mathrm{FT}(u_r)$ and $U_o = \mathrm{FT}(u_o)$. Howells et al. suggested that if a reference function u_r or its Fourier spectrum U_r is known, the object function u_o can be reconstructed through a deconvolution of the hologram I_{H} with U_r by using a Wiener filter [97]:

$$u_o = \mathrm{IFT}\left(I_{\mathrm{H}} \frac{U_r}{|U_r|^2 + \Phi} \right), \tag{23}$$

where Φ is the ratio of noise power to signal power and is usually treated as a constant, which is added to avoid having to divide by zero. He et al. employed this deconvolution approach to reconstruct a cluster of gold particles using another cluster of gold particles as a reference [98], and showed that the reconstruction obtained by applying a Wiener filter exhibits a poor quality. This poor quality, however, can be greatly improved by applying a few iterations, as shown in Figure 8.

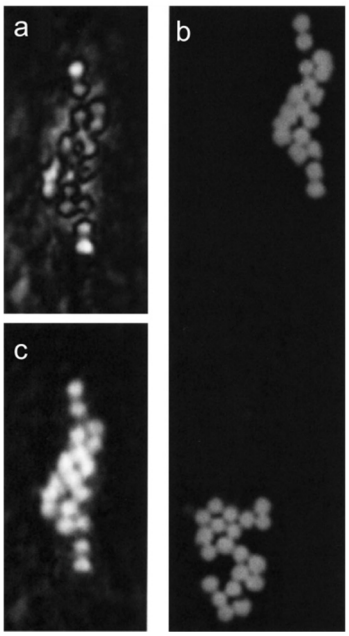

Figure 8. Fourier transform holography with arbitrary references. (**a**) Reconstruction of a cluster of gold balls from soft X-ray transmission diffraction patterns using deconvolution and a Wiener filter; one fast Fourier transform (FFT) was used. Constant $\Phi = 100$ in Equation (23) produced the best results. (**b**) Scanning electron microscopy image of the same cluster (upper one), the reference (lower one), and their relative positions. (**c**) Reconstruction obtained by using an iterative algorithm to reduce the effect of missing data due to a beam stop, 10 times FFT used. The diameter of each gold ball is about 50 nm. Reprinted from H. He, U. Weierstall, J. C. H. Spence, M. Howells, H. A. Padmore, S. Marchesini, H. N.Chapman, "Use of extended and prepared reference objects in experimental Fourier transform X-ray holography", Applied Physics Letters 85 (13), 2454–2456 (2004) [98], with the permission of AIP Publishing.

3.2.3.2. Reconstruction via System of Linear Equations

The presence of a known reference allows us to reformulate the reconstruction problem into a set of linear equations [92,99], as follows. The exit wave is given by Equation (1), and the IFT of the FT hologram by:

$$a(x,y) = a_o(x,y) + a_r(x,y) + c_{o,r}(x,y), \tag{24}$$

where $a_o(x,y)$ is the autocorrelation of the object wavefront, $a_r(x,y)$ is the autocorrelation of the reference wavefront, and $c_{o,r}(x,y)$ are the cross-correlations between the object and reference waves. When the object is finite, there are large regions of the autocorrelation function $a(x,y)$ where $a_o(x,y) = 0$. In these regions, Equation (24) can be reformulated as:

$$a(x,y) - a_r(x,y) = c_{o,r}(x,y) = Mu_o(x,y), \tag{25}$$

where the matrix M consists of the values of $u_r(x,y)$. Because both $a_r(x,y)$ and M are known, Equation (25) represents a system of linear equations for $u_o(x,y)$ which can be solved with an iterative linear retrieval using Fourier transforms (ILRUFT) [99]. An example of a reconstruction in which the reference was chosen in the shape of a 'cartoon cloud' [92] is shown in Figure 9.

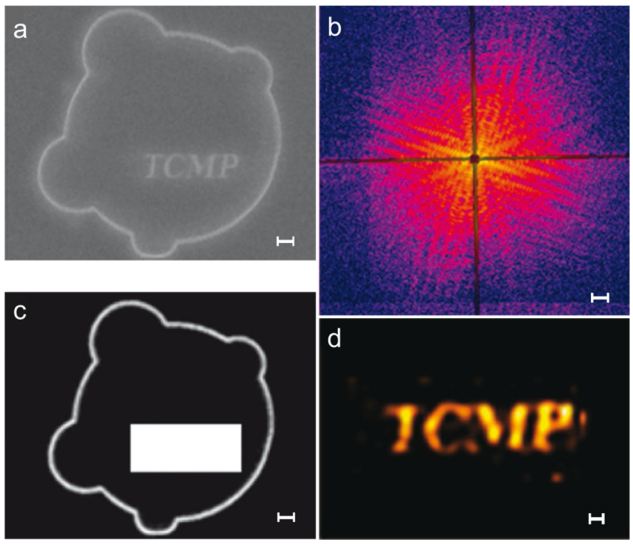

Figure 9. Holography with arbitrary references. (**a**) The scanning electron microscopy (SEM) image of the sample. (**b**) The corresponding diffraction pattern with central shaded areas indicating regions that have been set to zero for the reconstruction. (**c**) The reference function estimated from the SEM image along with the assumed object area indicated by the white rectangle. (**d**) The object intensity reconstructed with the iterative linear retrieval using Fourier transforms (ILRUFT) method. The scale bars in (**a**), (**c**), and (**d**) are 500 nm and the scale bar in (**b**) is 0.1 μm^{-1}. Reproduced from A. V. Martin, A. J. D'Alfonso, F. Wang, R. Bean, F. Capotondi, R. A. Kirian, E. Pedersoli, L. Raimondi, F. Stellato, C. H. Yoon, H. N. Chapman, "X-ray holography with a customizable reference", Nature Communications 5, 4661 (2014) [92], with permission from Springer Nature.

4. FTH with Different Types of Waves

4.1. Light

The first experimental demonstration of FTH was performed using a light-optical setup [11,12], and since then several studies have reported FTH with light [16–19,75,77,78,100–107]. However, FTH is not a popular choice for coherent imaging with light. FTH has no significant advantages over conventional optical imaging because of the availability of good-quality optical elements. Additionally, unlike conventional imaging with lenses, FTH requires a special sample arrangement and a careful setting of experimental conditions such as matching intensities between the object and reference waves. Yet, light-optical FTH is a top pick for testing novel or advanced forms of FTH [18,19,75,77], and for performing educational experiments [16], an example is shown in Figure 10. The sizes of objects imaged using light-optical FTH do not exceed a few millimetres. Typically, a laser beam with a diameter of 1–2 mm and a Gaussian intensity profile is expanded by using a pinhole and collimating lens system to create an illuminating beam with a larger diameter [16]. In order to minimise the size of the optical setup for FTH, a lens is typically placed after the sample to perform FT instead of a detector being placed in the far field, as shown in Figure 10 (lens C2). The detector should be placed behind the lens at the exact focal length of the lens. The focal length of the lens f defines the size of the reconstructed sample area, as given by Equation (15): $s_0 = \frac{\lambda f}{\Delta_X}$.

An interesting application of light-optical FTH is coloured 3D imaging [101], shown in Figure 11. In this scheme, red, green, and blue lasers were employed to record the FTH holograms of a 3D object. Like in off-axis holography arrangement, the laser beam here was split into two beams: the object and reference beams, where the reference beam is being expanded, as shown in Figure 11. To satisfy the requirements of FTH, the distance between the object and the CCD was set to be equal to that between the reference-point source and the CCD. For each wavelength, a monochromatic digital FT hologram was recorded. Then, the three corresponding reconstructed images were numerically treated

to become the same size. One of the advantages of FTH is that it allows for the precise superposition of reconstructed images onto one coloured 3D reconstruction.

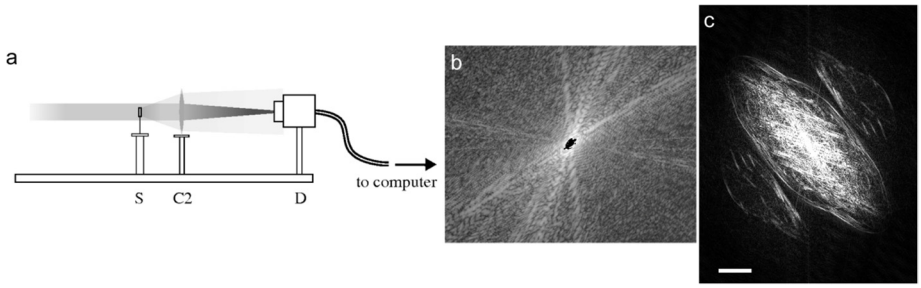

Figure 10. Fourier transform holography using light in an optical laboratory. (**a**) The detector part of the experimental setup. The collector lens C2 is placed downstream from the sample S. The charge-coupled device (CCD) detector D is placed at the back focal plane of the lens. The incident beam is focused on the CCD and the far-field diffraction pattern is formed in the CCD plane. (**b**) The recorded Fourier transform hologram, sampled with 489 × 508 pixels at a pixel size of 9.6 × 7.5 μm^2. (**c**) The autocorrelation of the sample distribution—an insect wing and a small additional scatterer (the presence of the small scatterer was not intentional), obtained using the Fourier transform of the hologram. The scalebar is 1 mm. Reproduced from P. Thibault, I. C. Rankenburg, "Optical diffraction microscopy in a teaching laboratory", American Journal of Physics 75 (9), 827–832 (2007) [16], with the permission of the American Association of Physics Teachers.

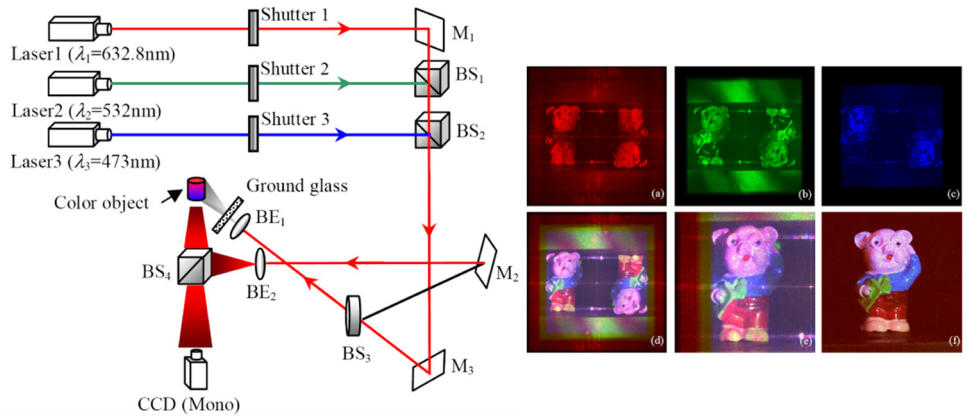

Figure 11. Three-dimensional coloured Fourier transform holography using light. Left: experimental scheme. M—mirror; BE—beam-expander; and BS—beam-splitter. Right: reconstructions of the hologram recorded with (**a**) λ_1 = 632.8 nm, (**b**) λ_2 = 532 nm, and (**c**) λ_3 = 473 nm. (**d**) Fused colour reconstructed object. (**e**) Part magnification of (**d**). (**f**) Photograph of the coloured object used in the experiment. Adapted from J. L. Zhao, H. Z. Jiang, J. L. Di, "Recording and reconstruction of a color holographic image by using digital lensless Fourier transform holography", Optics Express 16 (4), 2514–2519 (2008) [101], © 2008 Optica Publishing Group.

4.2. Electrons

Only a few studies have demonstrated FTH using electrons. One of the reasons for this is that state-of-the art aberration-corrected TEMs provide atomic-resolution images of samples. The other reason is that off-axis holography is a conventional choice for phase imaging with electrons [108,109]. Recently, Harada et al. employed an FTH-based imaging scheme for visualising phase vortices in an electron beam [110,111], shown in Figure 12. The object was a binary phase-shifting pattern in the form of a fork, shown in Figure 12b. Such a fork-like pattern is a hologram created by the interference of a wave with a phase vortex and a plane reference wave;he wave with the phase vortex is reconstructed when the hologramis illuminated with the plane reference wave [112]. In the experiments of Harada

et al., the fork-like pattern occupied only a small, central part of the sample area [110,111], shown in Figure 12c. When illuminated by a convergent electron beam, the part of the incident wave that did not interact with the object converged into a bright spot that served as the reference. The part of the incident wave that interacted with the object was scattered and created the first and higher order diffraction patterns, which served as objects. Thus, in this arrangement, the focal plane played the same role as the sample plane in conventional FTH. The hologram was then recorded in the far field (Figure 12d). Reconstructions were obtained by selecting a region in the hologram and calculating its FT [111].

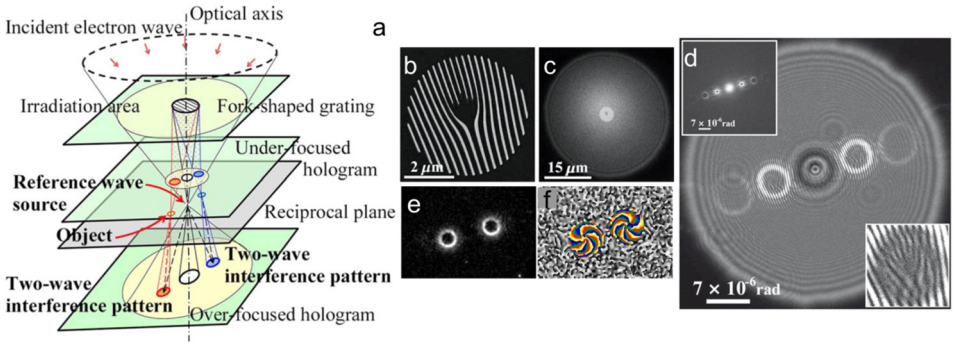

Figure 12. Imaging phase vortices in an electron beam using Fourier transform holography. (**a**) Experimental arrangement. (**b**) Fork-shaped pattern (grating) in a 150-nm-thick Si_3N_4 membrane with an intensity transmittance of about 44%. (**c**) Fork-shaped grating and the irradiation area of about 10 times the grating size for this electron holography. (**d**) Defocused small-angle electron diffraction (SmAED) pattern as exhibiting electron holograms of the fork-shaped grating. Four holograms on both sides of the optical axis are recorded in a single interferogram. The upper-left inset is the FT of the defocused SmAED pattern and the lower-right inset represents the enlarged interference pattern inside the ring-shaped spot of the right-hand side. (**e**,**f**) are the amplitude and phase distributions, respectively, of the vortex beams reconstructed from the first-order SmAED ring-shaped spots. Adapted from K. Harada, K. Shimada, Y. A. Ono, "Electron holography for vortex beams", Applied Physics Express 13 (3), 032003 (2020), doi: 10.35848/1882-0786/ab7059 [111].

4.3. X-rays and Extreme Ultraviolet

FTH with X-rays and extreme ultraviolet waves are discussed here in one section because of their somewhat overlapping wavelengths ranges: 0.1–10 nm for soft X-rays [20,22–33,35–37,40–42,47,49–51,54–59,61–63,68,69,72,73,79,80,83–86,88,89,91–93,97,98,113–128], less than 0.1 nm for hard X-rays [21,44,46,54,129,130], and 10–124 nm for extreme ultraviolet (XUV) waves [34,43,60,64–67,70,71,82,93,131]. As a lensless imaging technique, FTH is most often performed with X-rays where a lack of high quality optical elements prevents conventional focused imaging. For X-rays, a decoupling of the reference size and reference wave intensity can be achieved using a specially designed zone plate with a central opening to allow the central part of the beam to go unchanged and illuminate the object with a plane wave. The rest of the zone plate focuses the non-central part of the incident beam into a spot in the sample plane that serves as a reference [20], as sketched in Figure 13. A slightly different approach was proposed by Geilhufe et al., who showed that one can employ a mask containing both an object and Fresnel zone plate (FZP). This allows for the separation of the positions of reference source and object along the *z*-axis [121]. Recently, Pratch et al. demonstrated that a specially designed digital optical element (DOE) could simultaneously create object illumination and reference wave [127]. The following review papers are referred to for further reading about X-ray FTH [132–137].

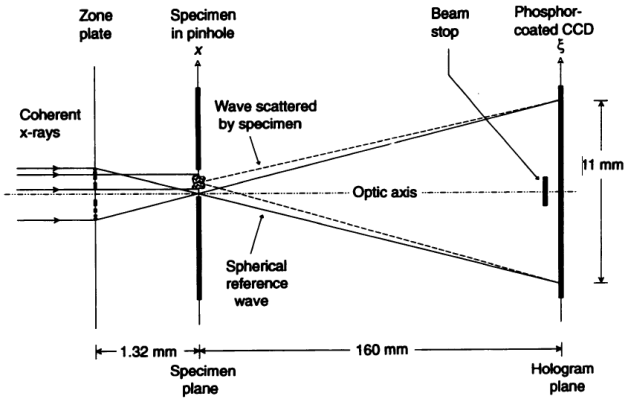

Figure 13. Fourier transform holography with soft X-rays. A coherent X-ray beam illuminates the zone plate (shown in profile). The undeviated wave illuminates the specimen, and the focused wave serves as a reference source. A charge-coupled device (CCD) detector records the interference between the specimen and reference waves. The X-rays that are not scattered by the specimen are blocked by the beam stop to prevent the saturation of the CCD. From I. McNulty, J. Kirz, C. Jacobsen, E. H. Anderson, M. R. Howells, D. P. Kern, "High-resolution imaging by Fourier-transform X-ray holography", Science 256 (5059), 1009–1012 (1992) [20]; Reprinted with permission from AAAS.

FTH is often performed using compact table-top sources [138] of coherent soft X-ray or XUV sources [34,36,47,62,64,70,71,79,82,86,131]. The object and reference arrangement of FTH performed using a table-top source is identical to that of FTH using synchrotron or free electron laser (FEL) source. The first demonstration of FTH using a table-top source was reported by Sandberg et al. in 2009, they performed FTH with multiple poin-tlike references and achieved a resolution of 53 nm using X-rays with wavelengths of 29 nm [47]. FTH using a table-top XUV laser with a 46.9 nm wavelength was first demonstrated by Malm et al. in 2013 [82].

5. X-ray FTH Applications

5.1. Imaging of Magnetic Domains—Spectro-Holography

Random magnetic domains in Co–Pt multilayer film were first imaged using soft X-ray FTH by Eisebitt et al. in 2004 [22], shown in Figure 14. In the reconstructed images, the amplitude contrast was given by X-ray magnetic circular dichroism (XMCD), which is a property of the materials that allows them to absorb X-rays to different extents based on whether the photon's helicity and the sample magnetisation are parallel or anti-parallel. Magnetic domains are often imaged by using mainly circular dichroism (XMCD) [29,61,64,83], and less often by using linear dichroism (XMLD) [27,59,63]. Because this imaging technique combines spectroscopy and holography, it is often named as spectro-holography and it is widely employed for imaging magnetic structures [22,24,27,29,30,33,48,51–54,56,59–61,63–67,69,72,73,81,83–85,88,89,93,115,118,122,123,125,128,129,139,140]. In particular, spectro-holography has been used to study such effects as the magnetisation distribution in materials that host topological phases such as skyrmions [88,89], as well as the nucleation, annihilation, and dynamics of skyrmions [69,72,73,122,128].

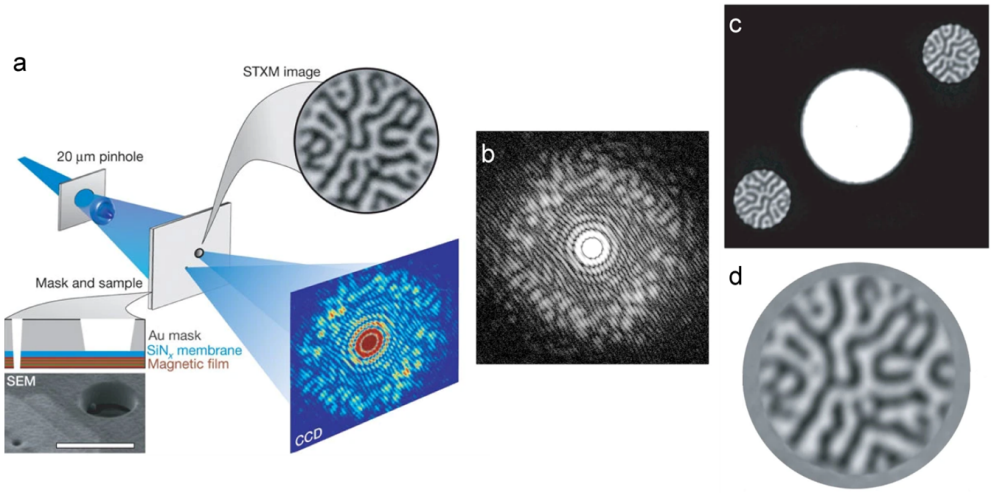

Figure 14. Fourier transform holography of a random magnetic domain structure in a Co–Pt multilayer film using soft X-rays (λ = 1.59 nm, E = 778 eV). (**a**) Scheme of the experimental setup. Monochromatised and circular polarised X-rays are illuminating the mask–sample structure after spatial coherence filtering. The object and reference beam are defined by the mask, and the resulting hologram is recorded on a CCD detector. The lower inset shows the geometry and a scanning electron microscopy (SEM) image of the sample structure. The scale bar in the SEM image is 2.0 µm. The top inset shows a scanning transmission X-ray microscopy (STXM) image of the magnetic structure illuminated through the sample aperture. The field of view is 1.5 µm. (**b**) Hologram recorded with right circular polarisation X-rays. Intensity is represented in a logarithmic grey scale. (**c**) Two-dimensional fast Fourier transformation of the hologram in (**b**). (**d**) Zoomed-in image, obtained by subtracting the Fourier transformations of opposite-helicity holograms, showing the magnetisation map of the sample; the diameter of the shown area is 1.5 µm. Reproduced from S. Eisebitt, J. Lüning, W. F. Schlotter, M. Lorgen, O. Hellwig, W. Eberhardt, J. Stohr, "Lensless imaging of magnetic nanostructures by X-ray spectro-holography", Nature 432 (7019), 885–888 (2004) [22], with permission from Springer Nature.

5.2. Time-Resolved Imaging

Both FELs and high-harmonic generation (HHG) sources produce coherent femtosecond X-ray pulses suitable for imaging with femtosecond temporal and nanometre spatial resolutions [28,33,43,71,117,119,125]. Although successive X-ray pulses in the femtosecond regime could be realised, the recording of femtosecond-delayed images still constitutes a challenge. As a step towards achieving a molecular movie, in 2011, Guenther et al. demonstrated a holographic imaging approach capable of recording two fully independent images with a variable time delay over the entire femtosecond regime [117]. Guenther et al. used two illuminating beams, and each beam illuminated the sample and a different set of point-like references. By calculating the FT of the recorded hologram, the object distributions were reconstructed at the position of the references. By knowing the time when the corresponding reference was illuminated, the time of the object acquisition was determined [117]. In 2014, Schmising et al. imaged the magnetisation dynamics within the magnetic domain of a Co–Pd layer, following the creation of a localised excitation using a pump-probe FTH by (or via) an optical standing wave with a temporal resolution of 100 fs and a spatial resolution of sub-100 nm [33]. In 2021, Zayko et al. stroboscopically traced the local magnetisation dynamics and localised spin structures in Co–Pd multilayers with sub-wavelength spatial resolutions of 16 nm and 40 fs temporal resolutions using a table-top high-harmonic generation setup (with a wavelength of 21 nm) [125], as shown in Figure 15.

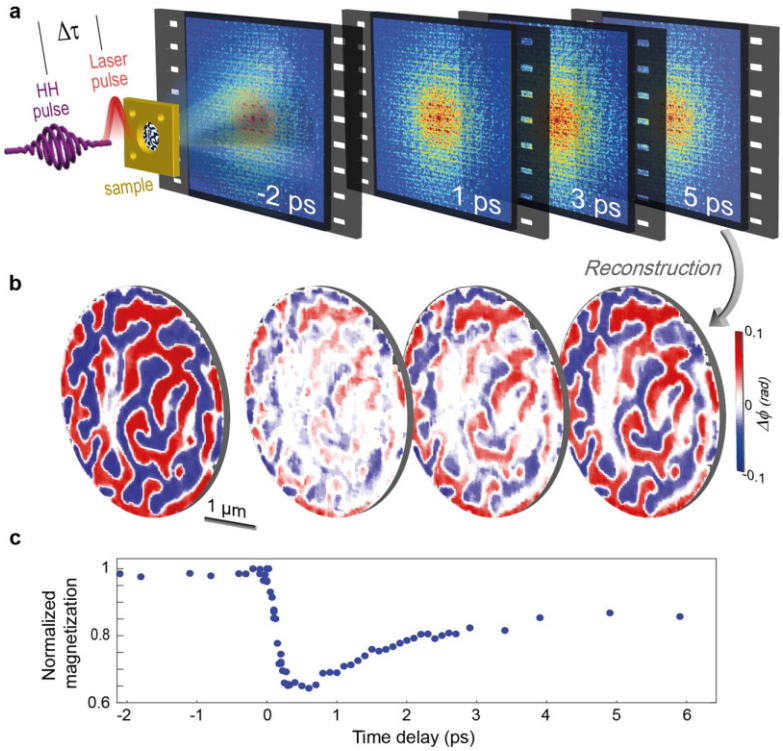

Figure 15. Ultrafast high-harmonic nanoscopy. (**a**) A magnetic sample (Co–Pd multilayers) is excited with a femtosecond laser pulse and probed with a circularly polarised high-harmonic pulse (with a wavelength of 21 nm) over a variable time delay. A quantitative real-space image is reconstructed from the diffraction pattern of the high-harmonic beam for each time delay between the pump and probe pulses. (**b**) The ratio of images obtained from opposite high-harmonic generation helicities provides a map of the magnetic contrast isolated from nonmagnetic contributions, i.e., femtosecond snapshot of the spin structures at a given time delay between pump and probe pulses. (**c**) Plot of the spatially averaged, normalised magnetisation within the field of view as a function of time delay. Adapted from S. Zayko, O. Kfir, M. Heigl, M. Lohmann, M. Sivis, M. Albrecht, M. C. Ropers, "Ultrafast high-harmonic nanoscopy of magnetization dynamics", Nature Communications 12 (1), 6337 (2021) [125].

5.3. Biological Imaging

Soft X-ray FTH has been applied for imaging biological objects such as diatoms [25,26,31,35,50] and mimiviruses [68]. Gorkhover et al. imaged individual mimivirus particles (450 nm in diameter) by using Xe clusters (30–120 nm in diameter) as references; the mimivirus particles and Xe clusters were shot onto the X-ray beam from two separate jets [68], as shown in Figure 16. Due to the relatively large wavelengths of soft X-rays, the resolution achieved in the reconstruction of FT holograms was in the order of a few tens of nanometre.

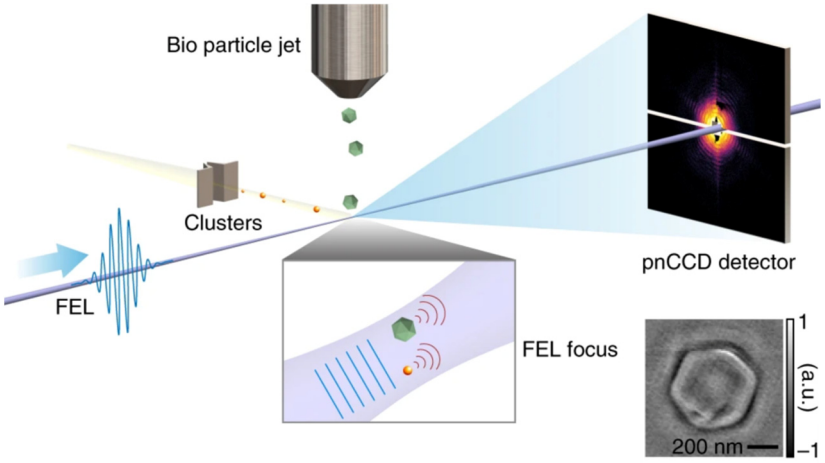

Figure 16. Femtosecond X-ray Fourier holography imaging of free-flying nanoparticles. The reconstruction of the mimivirus from the hologram is shown in the bottom right corner. Reproduced from T. Gorkhover, A. Ulmer, K. Ferguson, M. Bucher, F. Maia, J. Bielecki, T. Ekeberg, M. F. Hantke, B. J. Daurer, C. Nettelblad, J. Andreasson, A. Barty, P. Bruza, S. Carron, D. Hasse, J. Krzywinski, D. S. D. Larsson, A. Morgan, K. Muhlig, M. Muller, K. Okamoto, A. Pietrini, D. Rupp, M. Sauppe, G. van der Schot, M. Seibert, J. A. Sellberg, M. Svenda, M. Swiggers, N. Timneanu, D. Westphal, G. Williams, A. Zani, H. N. Chapman, G. Faigel, T. Moller, J. Hajdu, and C. Bostedt, "Femtosecond X-ray Fourier holography imaging of free-flying nanoparticles", Nature Photonics 12 (3), 150–155 (2018) [68], with permission from Springer Nature.

5.4. Three-Dimensional Imaging

Since FTH is a holographic technique, it provides access to 3D information in a single intensity measurement. The complex-valued exit wave distribution reconstructed from an FT hologram can be propagated using numerical algorithms [141] to obtain focused images of a sample [32,50,131]. However, wavefront propagation is only possible when the complex-valued exit wave is reconstructed using non-iterative algorithms, that is, via single FT. When an iterative method is applied, the resulting reconstruction is the object's (or sample's) projection and not the complex-valued exit wave. The possibility of restoring 3D information from a single FT hologram was investigated by Monserud et al. in 2014 [131]. The authors used an XUV table-top source (λ = 46.9 nm) and acquired FT holograms of three swaying pillars with a very short exposure time of 1.2 ns, which allowed them to capture the dynamic bending of the pillars. The three pillars were refocused during reconstruction and their 3D bending was visualised. Similar studies were reported by Geilhufe et al., who imaged a static nanofabricated structure with four equidistant height levels using soft X-rays (λ = 3.1 nm, E = 400 eV) and obtained a 3D reconstruction in the z-range of 9 µm [32] (Figure 17).

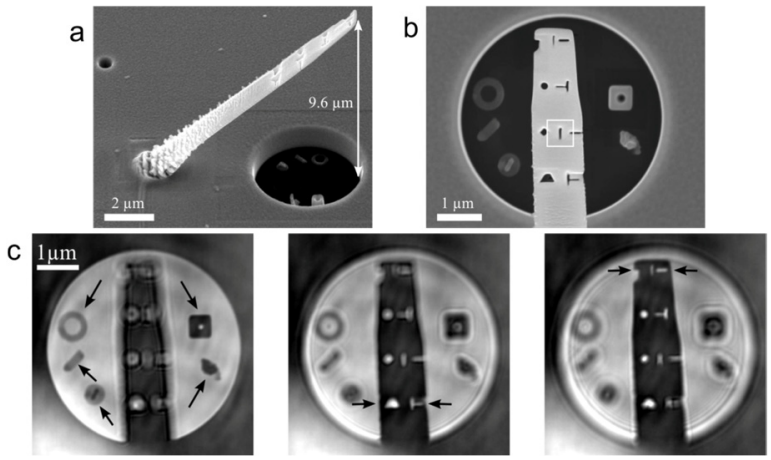

Figure 17. Extracting 3D information from a single X-ray Fourier transform hologram. (**a**,**b**) Scanning electron microscopy image of the test sample made from 3D platinum structures. The side view of the sample (**a**) shows the structured ramp which extends above the object hole. The ramp is deposited with a 45° inclination on a gold mask. The small pinhole seen on the upper left represents the reference source, whereas the large circular aperture seen at the bottom right constitutes the object's aperture. The top view (**b**) shows different platinum structures deposited on a Si_3N_4 membrane at the bottom of the object aperture. (**c**) Real part of the reconstructed object wave field corresponding to different longitudinal displacements from the substrate. The reconstruction on the left corresponds to the mask plane. The reconstructions shown in the middle and on the right are obtained by numerical propagation of the reconstructed wave field upstream by 6 µm and 9 µm, respectively. Focused features are indicated by the black arrows. Adapted from J. Geilhufe, C. Tieg, B. Pfau, C. M. Gunther, E. Guehrs, S. Schaffert, and S. Eisebitt, "Extracting depth information of 3-dimensional structures from a single-view X-ray Fourier-transform hologram", Optics Express 22 (21), 24959 – 24969 (2014) [32], © 2014 Optica Publishing Group.

6. FTH and Other Coherent Imaging Techniques

FTH arrangement is similar to an in-line or Gabor-type holography, as shown in Figure 18. In Gabor-type holography [2,3], an object is placed into a divergent wavefront and a hologram is formed by interference between the diffracted and non-diffracted waves. A serious drawback of Gabor holography is the so-called twin image, which always shows up in the reconstruction as being superimposed onto the reconstructed object distribution [3]; however, this problem can be solved by applying iterative methods [142,143]. A comparison between reconstructions obtained from experimental light-optical FTH and Gabor-type holograms was performed by Podorov et al. [75], as shown in Figure 18.

FTH has been performed in combination with scanning to increase the field of view [35,51], with tomography to obtain 3D-object reconstruction [31,144], and with ptychography to provide accurate information of the positions of the probing beam [35]. The separation of the optical elements for a reference and for an object-supporting mask provides new possibilities for arbitrarily shift or rotation of the imaged object. An example of such an arrangement, which enables scanning FTH, is shown in Figure 19.

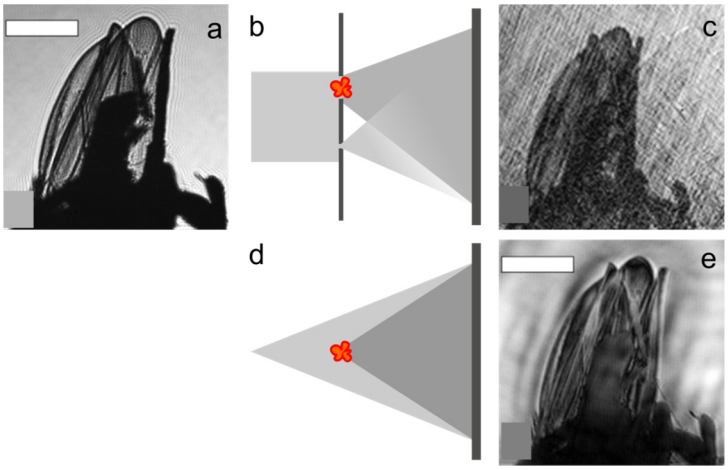

Figure 18. Comparison between reconstructions obtained from experimental light optical Fourier transform (FT) and Gabor-type holograms. (**a**) Direct optical image of the object (an Australian gnat placed on a rectangular based pyramid) obtained using a He–Ne laser source. (**b**) Arrangement for Fourier transform holography (FTH). (**c**) Magnitude of the reconstructed distribution obtained from the FT hologram. (**d**) Arrangement for Gabor in-line holography. (**e**) Image of the object reconstructed from the Gabor in-line hologram. Scale bar in (**a**,**e**) is 200 μm. Reprinted from S. G. Podorov, A. I. Bishop, D. M. Paganin, K. M. Pavlov, "Mask-assisted deterministic phase-amplitude retrieval from a single far-field intensity diffraction pattern: Two experimental proofs of principle using visible light", Ultramicroscopy 111 (7), 782–787 (2011) [75], with permission from Elsevier.

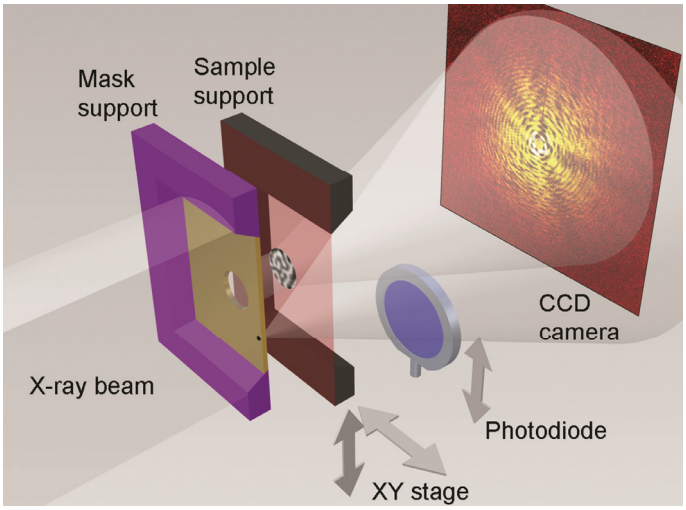

Figure 19. Schematic diagram of the X-ray holographic microscopy setup, consisting of a holography mask support, a movable object (sample) support, and a charge coupled device (CCD) detector. The membrane with the optical elements (mask), i.e., the object and reference holes, is fixed in the centre of the X-ray beam. A second membrane, which provides support for the object, can be moved freely in a plane perpendicular to the beam. Reprinted from D. Stickler, R. Fromter, H. Stillrich, C. Menk, C. Tieg, S. Streit-Nierobisch, M. Sprung, C. Gutt, L. M. Stadler, O. Leupold, G. Grubel, and H. P. Oepen, Applied Physics Letters 96 (4), 042501 (2010) [51], with the permission of AIP Publishing.

7. Conclusions

FTH has been continuously developed in both experimental and data analysis aspects. Various shapes of reference apertures have been proposed to increase the intensity of reference wave, comparing to the original FTH design with a single point-like reference. In X-ray FTH, zone plates and other DOEs were demonstrated for focusing incident beam

into a point-like reference, thus eliminating the requirement for a physical reference in the sample plane [20]; the point-like reference could even be created in a different plane than the sample one [121]. A large field of view or 3D-sample distribution can be imaged by separating the planes with optical elements (the reference and object supporting mask) and those with the object, allowing for the arbitrary shifting or rotating of the object [31,35,51,55].

Numerical algorithms have been developed to improve the quality of reconstructed object distributions and to reach the resolution given by the numerical aperture of the optical setup rather than by the size of the reference: iterative phase retrieval [16,23,30,35,37,43,44,47,57,64,70,71,78,80,92,98,116,126], compressive sensing [105], deconvolution [124], and, more recently, deep learning [19] algorithms. Future development can be expected from adapting the FTH principle to other than real space domain, for example, Fourier domain as shown by Harada et al. [111]. Novel FTH applications are anticipated from using bright, intense coherent ultra-short X-ray sources for time-resolved FTH at nanometre resolutions, and for imaging of biological samples [68].

Author Contributions: S.M. and T.L. both contributed equally to writing the manuscript. All authors have read and agreed to the published version of the manuscript.

Funding: This work was funded by the Swiss National Foundation Research Grant 200021_197107.

Institutional Review Board Statement: Not applicable.

Informed Consent Statement: Not applicable.

Data Availability Statement: The data that support the presented results are available from the corresponding author upon reasonable request.

Conflicts of Interest: The authors declare no conflict of interest.

References

1. Gabor, D. Improvements in and Relating to Microscopy. Patent The British Thomson-Houston Company. GB Patent 685,286, 17 December 1947.
2. Gabor, D. A new microscopic principle. *Nature* **1948**, *161*, 777–778. [CrossRef] [PubMed]
3. Gabor, D. Microscopy by reconstructed wave-fronts. *Proc. R. Soc. Lond. A* **1949**, *197*, 454–487. [CrossRef]
4. Miao, J.W.; Sayre, D.; Chapman, H.N. Phase retrieval from the magnitude of the Fourier transforms of nonperiodic objects. *J. Opt. Soc. Am. A* **1998**, *15*, 1662–1669. [CrossRef]
5. Miao, J.W.; Charalambous, P.; Kirz, J.; Sayre, D. Extending the methodology of X-ray crystallography to allow imaging of micrometre-sized non-crystalline specimens. *Nature* **1999**, *400*, 342–344. [CrossRef]
6. Miao, J.W.; Kirz, J.; Sayre, D. The oversampling phasing method. *Acta Crystall. D* **2000**, *56*, 1312–1315. [CrossRef]
7. Fienup, J.R. Phase retrieval algorithms—A comparison. *Appl. Opt.* **1982**, *21*, 2758–2769. [CrossRef]
8. Shechtman, Y.; Eldar, Y.C.; Cohen, O.; Chapman, H.N.; Miao, J.W.; Segev, M. Phase retrieval with application to optical imaging. *IEEE Signal Process. Mag.* **2015**, *32*, 87–109. [CrossRef]
9. Latychevskaia, T. Iterative phase retrieval in coherent diffractive imaging: Practical issues. *Appl. Opt.* **2018**, *57*, 7187–7197. [CrossRef]
10. Winthrop, J.T.; Worthington, C.R. X-ray microscopy by successive Fourier transformation. *Phys. Lett.* **1965**, *15*, 124–126. [CrossRef]
11. Stroke, G.W. Lensless Fourier-transform method for optical holography. *Appl. Phys. Lett.* **1965**, *6*, 201–203. [CrossRef]
12. Winthrop, J.T.; Worthington, C.R. X-ray microscopy by successive Fourier transformation 2. An optical analogue experiment. *Phys. Lett.* **1966**, *21*, 413–415. [CrossRef]
13. Wiener, N. Generalized harmonic analysis. *Acta Math.* **1930**, *55*, 117–258. [CrossRef]
14. Khintchin, A. Korrelationstheorie der stationären stochastischen Prozesse. *Math. Ann.* **1934**, *109*, 604–615. [CrossRef]
15. Debevec, P.E.; Malik, J. Recovering high dynamic range radiance maps from photographs. *Siggraph* **1997**, *130*, 1–10.
16. Thibault, P.; Rankenburg, I.C. Optical diffraction microscopy in a teaching laboratory. *Am. J. Phys.* **2007**, *75*, 827–832. [CrossRef]
17. DeVelis, J.B.; Raso, D.J.; Reynolds, G.O. Effect of source size on the resolution in Fourier-transform holography. *J. Opt. Soc. Am.* **1967**, *57*, 843–844. [CrossRef]
18. Zhang, J.Y.; Ren, Z.Y.; Zhu, J.Q.; Lin, Z.Q. Phase-shifting lensless Fourier-transform holography with a Chinese Taiji lens. *Opt. Lett.* **2018**, *43*, 4085–4087. [CrossRef]
19. Liao, M.H.; Feng, Y.L.; Lu, D.J.; Li, X.Y.; Pedrini, G.; Frenner, K.; Osten, W.; Peng, X.; He, W.Q. Scattering imaging as a noise removal in digital holography by using deep learning. *New J. Phys.* **2022**, *24*, 083014. [CrossRef]
20. McNulty, I.; Kirz, J.; Jacobsen, C.; Anderson, E.H.; Howells, M.R.; Kern, D.P. High-resolution imaging by Fourier-transform X-ray holography. *Science* **1992**, *256*, 1009–1012. [CrossRef]

21. Leitenberger, W.; Snigirev, A. Microscopic imaging with high energy X-rays by Fourier transform holography. *J. Appl. Phys.* **2001**, *90*, 538–544. [CrossRef]
22. Eisebitt, S.; Luning, J.; Schlotter, W.F.; Lorgen, M.; Hellwig, O.; Eberhardt, W.; Stohr, J. Lensless imaging of magnetic nanostructures by X-ray spectro-holography. *Nature* **2004**, *432*, 885–888. [CrossRef] [PubMed]
23. Eisebitt, S.; Lorgen, M.; Eberhardt, W.; Luning, J.; Andrews, S.; Stohr, J. Scalable approach for lensless imaging at X-ray wavelengths. *Appl. Phys. Lett.* **2004**, *84*, 3373–3375. [CrossRef]
24. Gunther, C.M.; Radu, F.; Menzel, A.; Eisebitt, S.; Schlotter, W.F.; Rick, R.; Luning, J.; Hellwig, O. Steplike versus continuous domain propagation in Co/Pd multilayer films. *Appl. Phys. Lett.* **2008**, *93*, 072505. [CrossRef]
25. Guehrs, E.; Gunther, C.M.; Konnecke, R.; Pfau, B.; Eisebitt, S. Holographic soft X-ray omni-microscopy of biological specimens. *Opt. Express* **2009**, *17*, 6710–6720. [CrossRef] [PubMed]
26. Mancuso, A.P.; Gorniak, T.; Staler, F.; Yefanov, O.M.; Barth, R.; Christophis, C.; Reime, B.; Gulden, J.; Singer, A.; Pettit, M.E.; et al. Coherent imaging of biological samples with femtosecond pulses at the free-electron laser FLASH. *New J. Phys.* **2010**, *12*, 035003. [CrossRef]
27. Pfau, B.; Gunther, C.M.; Konnecke, R.; Guehrs, E.; Hellwig, O.; Schlotter, W.F.; Eisebitt, S. Magnetic imaging at linearly polarized X-ray sources. *Opt. Express* **2010**, *18*, 13608–13615. [CrossRef]
28. Pfau, B.; Gunther, C.M.; Schaffert, S.; Mitzner, R.; Siemer, B.; Roling, S.; Zacharias, H.; Kutz, O.; Rudolph, I.; Treusch, R.; et al. Femtosecond pulse X-ray imaging with a large field of view. *New J. Phys.* **2010**, *12*, 095006. [CrossRef]
29. Pfau, B.; Gunther, C.M.; Guehrs, E.; Hauet, T.; Yang, H.; Vinh, L.; Xu, X.; Yaney, D.; Rick, R.; Eisebitt, S.; et al. Origin of magnetic switching field distribution in bit patterned media based on pre-patterned substrates. *Appl. Phys. Lett.* **2011**, *99*, 062502. [CrossRef]
30. Flewett, S.; Gunther, C.M.; Schmising, C.V.; Pfau, B.; Mohanty, J.; Buttner, F.; Riemeier, M.; Hantschmann, M.; Klaui, M.; Eisebitt, S. Holographically aided iterative phase retrieval. *Opt. Express* **2012**, *20*, 29210–29216. [CrossRef]
31. Guehrs, E.; Stadler, A.M.; Flewett, S.; Frommel, S.; Geilhufe, J.; Pfau, B.; Rander, T.; Schaffert, S.; Buldt, G.; Eisebitt, S. Soft X-ray tomoholography. *New J. Phys.* **2012**, *14*, 013022. [CrossRef]
32. Geilhufe, J.; Tieg, C.; Pfau, B.; Gunther, C.M.; Guehrs, E.; Schaffert, S.; Eisebitt, S. Extracting depth information of 3-dimensional structures from a single-view X-ray Fourier-transform hologram. *Opt. Express* **2014**, *22*, 24959–24969. [CrossRef]
33. Schmising, C.V.; Pfau, B.; Schneider, M.; Gunther, C.M.; Giovannella, M.; Perron, J.; Vodungbo, B.; Muller, L.; Capotondi, F.; Pedersoli, E.; et al. Imaging ultrafast demagnetization dynamics after a spatially localized optical excitation. *Phys. Rev. Lett.* **2014**, *112*, 217203. [CrossRef]
34. Williams, G.O.; Gonzalez, A.I.; Kunzel, S.; Li, L.; Lozano, M.; Oliva, E.; Iwan, B.; Daboussi, S.; Boutu, W.; Merdji, H.; et al. Fourier transform holography with high harmonic spectra for attosecond imaging applications. *Opt. Lett.* **2015**, *40*, 3205–3208. [CrossRef]
35. Hessing, P.; Pfau, B.; Guehrs, E.; Schneider, M.; Shemilt, L.; Geilhufe, J.; Eisebitt, S. Holography-guided ptychography with soft X-rays. *Opt. Express* **2016**, *24*, 1840–1851. [CrossRef]
36. Wang, S.J.; Rockwood, A.; Wang, Y.; Chao, W.L.; Naulleau, P.; Song, H.Y.; Menoni, C.S.; Marconi, M.; Rocca, J.J. Single-shot large field of view Fourier transform holography with a picosecond plasma-based soft X-ray laser. *Opt. Express* **2020**, *28*, 35898–35909. [CrossRef]
37. Malm, E.; Pfau, B.; Schneider, M.; Gunther, C.M.; Hessing, P.; Buttner, F.; Mikkelsen, A.; Eisebitt, S. Reference shape effects on Fourier transform holography. *Opt. Express* **2022**, *30*, 38424–38438. [CrossRef]
38. Blackledge, J.M.; Burge, R.E.; Hopcraft, K.I. The diffraction of plane waves from a circularly symmetrical aperture of finite thickness. *Optik* **1986**, *74*, 94–98.
39. Roberts, A. Electromagnetic theory of diffraction by a circular aperture in a thick, perfectly conducting screen. *J. Opt. Soc. Am. A Opt. Image Sci. Vis.* **1987**, *4*, 1970–1983. [CrossRef]
40. Schlotter, W.F.; Rick, R.; Chen, K.; Scherz, A.; Stohr, J.; Luning, J.; Eisebitt, S.; Gunther, C.; Eberhardt, W.; Hellwig, O.; et al. Multiple reference Fourier transform holography with soft X-rays. *Appl. Phys. Lett.* **2006**, *89*, 163112. [CrossRef]
41. Schlotter, W.F.; Luening, J.; Rick, R.; Chen, K.; Scherz, A.; Eisebitt, S.; Guenther, C.M.; Eberhardt, W.; Hellwig, O.; Stohr, J. Extended field of view soft X-ray Fourier transform holography: Toward imaging ultrafast evolution in a single shot. *Opt. Lett.* **2007**, *32*, 3110–3112. [CrossRef]
42. Sacchi, M.; Spezzani, C.; Carpentiero, A.; Prasciolu, M.; Delaunay, R.; Luning, J.; Polack, F. Experimental setup for lensless imaging via soft X-ray resonant scattering. *Rev. Sci. Instrum.* **2007**, *78*, 043702. [CrossRef] [PubMed]
43. Barty, A.; Boutet, S.; Bogan, M.J.; Hau-Riege, S.; Marchesini, S.; Sokolowski-Tinten, K.; Stojanovic, N.; Tobey, R.; Ehrke, H.; Cavalleri, A.; et al. Ultrafast single-shot diffraction imaging of nanoscale dynamics. *Nature Photon.* **2008**, *2*, 415–419. [CrossRef]
44. Stadler, L.M.; Gutt, C.; Autenrieth, T.; Leupold, O.; Rehbein, S.; Chushkin, Y.; Grubel, G. Hard X ray holographic diffraction imaging. *Phys. Rev. Lett.* **2008**, *100*, 245503. [CrossRef] [PubMed]
45. Eisebitt, S. X-ray holography—The hole story. *Nature Photon.* **2008**, *2*, 529–530. [CrossRef]
46. Stadler, L.M.; Gutt, C.; Autenrieth, T.; Leupold, O.; Rehbein, S.; Chushkin, Y.; Grubel, G. Fourier transform holography in the context of coherent diffraction imaging with hard X-rays. *Phys. Status Solidi A* **2009**, *206*, 1846–1849. [CrossRef]
47. Sandberg, R.L.; Raymondson, D.A.; La-o-Vorakiat, C.; Paul, A.; Raines, K.S.; Miao, J.; Murnane, M.M.; Kapteyn, H.C.; Schlotter, W.F. Tabletop soft-X-ray Fourier transform holography with 50 nm resolution. *Opt. Lett.* **2009**, *34*, 1618–1620. [CrossRef]

48. Streit-Nierobisch, S.; Stickler, D.; Gutt, C.; Stadler, L.M.; Stillrich, H.; Menk, C.; Fromter, R.; Tieg, C.; Leupold, O.; Oepen, H.P.; et al. Magnetic soft X-ray holography study of focused ion beam-patterned Co/Pt multilayers. *J. Appl. Phys.* **2009**, *106*, 083909. [CrossRef]
49. Tieg, C.; Fromter, R.; Stickler, D.; Stillrich, H.; Menk, C.; Streit-Nierobisch, S.; Stadler, L.M.; Gutt, C.; Leupold, O.; Sprung, M.; et al. Overcoming the Field-Of-View Restrictions in Soft X-Ray Holographic Imaging. In Proceedings of the 2nd Workshop on Polarized Neutrons and Synchrotron X-Rays for Magnetism, Bonn, Germany, 2–5 August 2009; IOP Publishing Ltd: Bonn, Germany, 2009; p. 012024.
50. Guehrs, E.; Gunther, C.M.; Pfau, B.; Rander, T.; Schaffert, S.; Schlotter, W.F.; Eisebitt, S. Wavefield back-propagation in high-resolution X-ray holography with a movable field of view. *Opt. Express* **2010**, *18*, 18922–18931. [CrossRef]
51. Stickler, D.; Fromter, R.; Stillrich, H.; Menk, C.; Tieg, C.; Streit-Nierobisch, S.; Sprung, M.; Gutt, C.; Stadler, L.M.; Leupold, O.; et al. Soft X-ray holographic microscopy. *Appl. Phys. Lett.* **2010**, *96*, 042501. [CrossRef]
52. Tieg, C.; Fromter, R.; Stickler, D.; Hankemeier, S.; Kobs, A.; Streit-Nierobisch, S.; Gutt, C.; Grubel, G.; Oepen, H.P. Imaging the in-plane magnetization in a Co microstructure by Fourier transform holography. *Opt. Express* **2010**, *18*, 27251–27256. [CrossRef]
53. Tieg, C.; Jimenez, E.; Camarero, J.; Vogel, J.; Arm, C.; Rodmacq, B.; Gautier, E.; Auffret, S.; Delaup, B.; Gaudin, G.; et al. Imaging and quantifying perpendicular exchange biased systems by soft X-ray holography and spectroscopy. *Appl. Phys. Lett.* **2010**, *96*, 072503. [CrossRef]
54. Awaji, N.; Nomura, K.; Doi, S.; Isogami, S.; Tsunoda, M.; Kodama, K.; Suzuki, M.; Nakamura, T. Large area imaging by Fourier transform holography using soft and hard X-rays. *Appl. Phys. Express* **2010**, *3*, 085201. [CrossRef]
55. Nomura, K.; Awaji, N.; Doi, S.; Isogami, S.; Kodama, K.; Nakamura, T.; Suzuki, M.; Tsunoda, M. Development of Scanning-Type X-Ray Fourier Transform Holography. In Proceedings of the 10th International Conference on X-ray Microscopy, Chicago, IL, USA, 15–20 August 2010; American Institute of Physics: Chicago, IL, USA, 2010; pp. 277–280.
56. Camarero, J.; Jimenez, E.; Vogel, J.; Tieg, C.; Perna, P.; Bollero, A.; Yakhou-Harris, F.; Arm, C.; Rodmacq, B.; Gautier, E.; et al. Exploring the limits of soft X-ray magnetic holography: Imaging magnetization reversal of buried interfaces (invited). *J. Appl. Phys.* **2011**, *109*, 07d357. [CrossRef]
57. Roy, S.; Parks, D.; Seu, K.A.; Su, R.; Turner, J.J.; Chao, W.; Anderson, E.H.; Cabrini, S.; Kevan, S.D. Lensless X-ray imaging in reflection geometry. *Nat. Photon.* **2011**, *5*, 243–245. [CrossRef]
58. Kim, H.T.; Kim, I.J.; Kim, C.M.; Jeong, T.M.; Yu, T.J.; Lee, S.K.; Sung, J.H.; Yoon, J.W.; Yun, H.; Jeon, S.C.; et al. Single-shot nanometer-scale holographic imaging with laser-driven X-ray laser. *Appl. Phys. Lett.* **2011**, *98*, 121105. [CrossRef]
59. Sacchi, M.; Popescu, H.; Jaouen, N.; Tortarolo, M.; Fortuna, F.; Delaunay, R.; Spezzani, C. Magnetic imaging by Fourier transform holography using linearly polarized X-rays. *Opt. Express* **2012**, *20*, 9769–9776. [CrossRef]
60. Capotondi, F.; Pedersoli, E.; Mahne, N.; Menk, R.H.; Passos, G.; Raimondi, L.; Svetina, C.; Sandrin, G.; Zangrando, M.; Kiskinova, M.; et al. Invited Article: Coherent imaging using seeded free-electron laser pulses with variable polarization: First results and research opportunities. *Rev. Sci. Instrum.* **2013**, *84*, 051301. [CrossRef]
61. Spezzani, C.; Popescu, H.; Fortuna, F.; Delaunay, R.; Breitwieser, R.; Jaouen, N.; Tortarolo, M.; Eddrief, M.; Vidal, F.; Etgens, V.H.; et al. Soft X-ray magneto-optics: Probing magnetism by resonant scattering experiments. *IEEE Trans. Magn.* **2013**, *49*, 4711–4716. [CrossRef]
62. Lee, K.H.; Yun, H.; Sung, J.H.; Lee, S.K.; Lee, H.W.; Kim, H.T.; Nam, C.H. Autocorrelation-subtracted Fourier transform holography method for large specimen imaging. *Appl. Phys. Lett.* **2015**, *106*, 061103. [CrossRef]
63. Wu, B.; Wang, T.; Graves, C.E.; Zhu, D.; Schlotter, W.F.; Turner, J.J.; Hellwig, O.; Chen, Z.; Durr, H.A.; Scherz, A.; et al. Elimination of X-ray diffraction through stimulated X-ray transmission. *Phys. Rev. Lett.* **2016**, *117*, 027401. [CrossRef]
64. Kfir, O.; Zayko, S.; Nolte, C.; Sivis, M.; Moller, M.; Hebler, B.; Arekapudi, S.; Steil, D.; Schafer, S.; Albrecht, M.; et al. Nanoscale magnetic imaging using circularly polarized high-harmonic radiation. *Sci. Adv.* **2017**, *3*, eaao4641. [CrossRef] [PubMed]
65. Willems, F.; Schmising, C.V.; Weder, D.; Gunther, C.M.; Schneider, M.; Pfau, B.; Meise, S.; Guehrs, E.; Geilhufe, J.; Merhe, A.E.; et al. Multi-color imaging of magnetic Co/Pt heterostructures. *Struct. Dyn.-US* **2017**, *4*, 014301. [CrossRef] [PubMed]
66. Schmising, C.V.; Weder, D.; Noll, T.; Pfau, B.; Hennecke, M.; Struber, C.; Radu, I.; Schneider, M.; Staeck, S.; Gunther, C.M.; et al. Generating circularly polarized radiation in the extreme ultraviolet spectral range at the free-electron laser FLASH. *Rev. Sci. Instrum.* **2017**, *88*, 053903.
67. Weder, D.; Schmising, C.V.; Willems, F.; Gunther, C.M.; Schneider, M.; Pfau, B.; Merhe, A.; Jal, E.; Vodungbo, B.; Luning, J.; et al. Multi-color imaging of magnetic Co/Pt multilayers. *IEEE Trans. Magn.* **2017**, *53*, 6500905. [CrossRef]
68. Gorkhover, T.; Ulmer, A.; Ferguson, K.; Bucher, M.; Maia, F.; Bielecki, J.; Ekeberg, T.; Hantke, M.F.; Daurer, B.J.; Nettelblad, C.; et al. Femtosecond X-ray Fourier holography imaging of free-flying nanoparticles. *Nat. Photon.* **2018**, *12*, 150–155. [CrossRef]
69. Caretta, L.; Mann, M.; Buttner, F.; Ueda, K.; Pfau, B.; Gunther, C.M.; Hessing, P.; Churikoval, A.; Klose, C.; Schneider, M.; et al. Fast current-driven domain walls and small skyrmions in a compensated ferrimagnet. *Nat. Nanotechnol.* **2018**, *13*, 1154–1161. [CrossRef]
70. Tadesse, G.K.; Eschen, W.; Klas, R.; Hilbert, V.; Schelle, D.; Nathanael, A.; Zilk, M.; Steinert, M.; Schrempel, F.; Pertsch, T.; et al. High resolution XUV Fourier transform holography on a table top. *Sci. Rep.* **2018**, *8*, 8677. [CrossRef]
71. Eschen, W.; Wang, S.C.; Liu, C.; Klas, R.; Steinert, M.; Yulin, S.; Meissner, H.; Bussmann, M.; Pertsch, T.; Limpert, J.; et al. Towards attosecond imaging at the nanoscale using broadband holography-assisted coherent imaging in the extreme ultraviolet. *Commun. Phys.* **2021**, *4*, 154. [CrossRef]

72. Buttner, F.; Pfau, B.; Bottcher, M.; Schneider, M.; Mercurio, G.; Gunther, C.M.; Hessing, P.; Klose, C.; Wittmann, A.; Gerlinger; et al. Observation of fluctuation-mediated picosecond nucleation of a topological phase. *Nat. Mater.* **2021**, *20*, 30–37. [CrossRef]
73. Gerlinger, K.; Pfau, B.; Buttner, F.; Schneider, M.; Kern, L.M.; Fuchs, J.; Engel, D.; Gunther, C.M.; Huang, M.T.; Lemesh, I.; et al. Application concepts for ultrafast laser-induced skyrmion creation and annihilation. *Appl. Phys. Lett.* **2021**, *118*, 192403. [CrossRef]
74. Podorov, S.G.; Pavlov, K.M.; Paganin, D.M. A non-iterative reconstruction method for direct and unambiguous coherent diffractive imaging. *Opt. Express* **2007**, *15*, 9954–9962. [CrossRef]
75. Podorov, S.G.; Bishop, A.I.; Paganin, D.M.; Pavlov, K.M. Mask-assisted deterministic phase-amplitude retrieval from a single far-field intensity diffraction pattern: Two experimental proofs of principle using visible light. *Ultramicroscopy* **2011**, *111*, 782–787. [CrossRef]
76. Guizar-Sicairos, M.; Fienup, J.R. Holography with extended reference by autocorrelation linear differential operation. *Opt. Express* **2007**, *15*, 17592–17612. [CrossRef]
77. Guizar-Sicairos, M.; Fienup, J.R. Direct image reconstruction from a Fourier intensity pattern using HERALDO. *Opt. Lett.* **2008**, *33*, 2668–2670. [CrossRef]
78. Tenner, V.T.; Eikema, K.S.E.; Witte, S. Fourier transform holography with extended references using a coherent ultra-broadband light source. *Opt. Express* **2014**, *22*, 25397–25409. [CrossRef]
79. Gauthier, D.; Guizar-Sicairos, M.; Ge, X.; Boutu, W.; Carre, B.; Fienup, J.R.; Merdji, H. Single-shot femtosecond X-ray holography using extended references. *Phys. Rev. Lett.* **2010**, *105*, 093901. [CrossRef]
80. Zhu, D.L.; Guizar-Sicairos, M.; Wu, B.; Scherz, A.; Acremann, Y.; Tyliszczak, T.; Fischer, P.; Friedenberger, N.; Ollefs, K.; Farle, M.; et al. High-resolution X-ray lensless imaging by differential holographic encoding. *Phys. Rev. Lett.* **2010**, *105*, 043901. [CrossRef]
81. Duckworth, T.A.; Ogrin, F.; Dhesi, S.S.; Langridge, S.; Whiteside, A.; Moore, T.; Beutier, G.; van der Laan, G. Magnetic imaging by X-ray holography using extended references. *Opt. Express* **2011**, *19*, 16223–16228. [CrossRef]
82. Malm, E.B.; Monserud, N.C.; Brown, C.G.; Wachulak, P.W.; Xu, H.W.; Balakrishnan, G.; Chao, W.L.; Anderson, E.; Marconi, M.C. Tabletop single-shot extreme ultraviolet Fourier transform holography of an extended object. *Opt. Express* **2013**, *21*, 9959–9966. [CrossRef]
83. Duckworth, T.A.; Ogrin, F.Y.; Beutier, G.; Dhesi, S.S.; Cavill, S.A.; Langridge, S.; Whiteside, A.; Moore, T.; Dupraz, M.; Yakhou, F.; et al. Holographic imaging of interlayer coupling in Co/Pt/NiFe. *New J. Phys.* **2013**, *15*, 023045. [CrossRef]
84. Spezzani, C.; Fortuna, F.; Delaunay, R.; Popescu, H.; Sacchi, M. X-ray holographic imaging of magnetic order in patterned Co/Pd multilayers. *Phys. Rev. B* **2013**, *88*, 224420. [CrossRef]
85. Liu, T.M.; Wang, T.H.; Reid, A.H.; Savoini, M.; Wu, X.F.; Koene, B.; Granitzka, P.; Graves, C.E.; Higley, D.J.; Chen, Z.; et al. Nanoscale confinement of all-optical magnetic switching in TbFeCo—Competition with nanoscale heterogeneity. *Nano Lett.* **2015**, *15*, 6862–6868. [CrossRef] [PubMed]
86. Boutu, W.; Gauthier, D.; Ge, X.; Cassin, R.; Ducousso, M.; Gonzalez, A.I.; Iwan, B.; Samaan, J.; Wang, F.; Kovacev, M.; et al. Impact of noise in holography with extended references in the low signal regime. *Opt. Express* **2016**, *24*, 6318–6327. [CrossRef] [PubMed]
87. Burgos-Parra, E.; Bukin, N.; Sani, S.; Figueroa, A.I.; Beutier, G.; Dupraz, M.; Chung, S.; Dürrenfeld, P.; Le, Q.T.; Mohseni, S.M.; et al. Investigation of magnetic droplet solitons using X-ray holography with extended references. *Sci. Rep.* **2018**, *8*, 11533. [CrossRef] [PubMed]
88. Ukleev, V.; Yamasaki, Y.; Morikawa, D.; Karube, K.; Shibata, K.; Tokunaga, Y.; Okamura, Y.; Amemiya, K.; Valvidares, M.; Nakao, H.; et al. Element-specific soft X-ray spectroscopy, scattering, and imaging studies of the skyrmion-hosting compound Co8Zn8Mn4. *Phys. Rev. B* **2019**, *99*, 144408. [CrossRef]
89. Turnbull, L.A.; Birch, M.T.; Laurenson, A.; Bukin, N.; Burgos-Parra, E.O.; Popescu, H.; Wilson, M.N.; Stefancic, A.; Balakrishnan, G.; Ogrin, F.Y.; et al. Tilted X-ray holography of magnetic bubbles in MnNiGa lamellae. *ACS Nano* **2021**, *15*, 387–395. [CrossRef]
90. Fenimore, E.E.; Cannon, T.M. Coded aperture imaging with uniformly redundant arrays. *Appl. Opt.* **1978**, *17*, 337–347. [CrossRef]
91. Marchesini, S.; Boutet, S.; Sakdinawat, A.E.; Bogan, M.J.; Bajt, S.; Barty, A.; Chapman, H.N.; Frank, M.; Hau-Riege, S.P.; Szoke, A.; et al. Massively parallel X-ray holography. *Nature Photon.* **2008**, *2*, 560–563. [CrossRef]
92. Martin, A.V.; D'Alfonso, A.J.; Wang, F.; Bean, R.; Capotondi, F.; Kirian, R.A.; Pedersoli, E.; Raimondi, L.; Stellato, F.; Yoon, C.H.; et al. X-ray holography with a customizable reference. *Nat. Commun.* **2014**, *5*, 4661. [CrossRef]
93. Gunther, C.M.; Guehrs, E.; Schneider, M.; Pfau, B.; Schmising, C.V.; Geilhufe, J.; Schaffert, S.; Eisebitt, S. Experimental evaluation of signal-to-noise in spectro-holography via modified uniformly redundant arrays in the soft X-ray and extreme ultraviolet spectral regime. *J. Opt.* **2017**, *19*, 064002. [CrossRef]
94. Fenimore, E.E.; Weston, G.S. Fast delta-Hadamard transform. *Appl. Opt.* **1981**, *20*, 3058–3067. [CrossRef]
95. Marchesini, S.; He, H.; Chapman, H.N.; Hau-Riege, S.P.; Noy, A.; Howells, M.R.; Weierstall, U.; Spence, J.C.H. X-ray image reconstruction from a diffraction pattern alone. *Phys. Rev. B* **2003**, *68*, 140101. [CrossRef]
96. Marchesini, S. A unified evaluation of iterative projection algorithms for phase retrieval. *Rev. Sci. Instrum.* **2007**, *78*, 011301. [CrossRef]
97. Howells, M.R.; Jacobsen, C.J.; Marchesini, S.; Miller, S.; Spence, J.C.H.; Weirstall, U. Toward a practical X-ray Fourier holography at high resolution. *Nucl. Instrum. Methods Phys. Res. Sect. A Accel. Spectrometers Detect. Assoc. Equip.* **2001**, *467*, 864–867. [CrossRef]
98. He, H.; Weierstall, U.; Spence, J.C.H.; Howells, M.; Padmore, H.A.; Marchesini, S.; Chapman, H.N. Use of extended and prepared reference objects in experimental Fourier transform X-ray holography. *Appl. Phys. Lett.* **2004**, *85*, 2454–2456. [CrossRef]

99. D'Alfonso, A.J.; Morgan, A.J.; Martin, A.V.; Quiney, H.M.; Allen, L.J. Fast deterministic approach to exit-wave reconstruction. *Phys. Rev. A* **2012**, *85*, 013816. [CrossRef]
100. Gaskill, J.D.; Goodman, J.W. Use of multiple reference sources to increase the effective field of view in lensless Fourier-transform holography. *Proc. IEEE* **1969**, *57*, 823–825. [CrossRef]
101. Zhao, J.L.; Jiang, H.Z.; Di, J.L. Recording and reconstruction of a color holographic image by using digital lensless Fourier transform holography. *Opt. Express* **2008**, *16*, 2514–2519. [CrossRef]
102. He, K.; Sharma, M.K.; Cossairt, O. High dynamic range coherent imaging using compressed sensing. *Opt. Express* **2015**, *23*, 30904–30916. [CrossRef]
103. Leshem, B.; Xu, R.; Dallal, Y.; Miao, J.W.; Nadler, B.; Oron, D.; Dudovich, N.; Raz, O. Direct single-shot phase retrieval from the diffraction pattern of separated objects. *Nat. Commun.* **2016**, *7*, 10820. [CrossRef]
104. Singh, R.K.; Vyas, S.; Miyamoto, Y. Lensless Fourier transform holography for coherence waves. *J. Opt.* **2017**, *19*, 115705. [CrossRef]
105. Vetal, A.P.; Singh, D.; Singh, R.K.; Mishra, D. Reconstruction of apertured Fourier Transform Hologram using compressed sensing. *Opt. Lasers Eng.* **2018**, *111*, 227–235. [CrossRef]
106. Xie, J.; Zhang, J.Y.; Pan, X.; Zhou, S.L.; Ma, W.X. Multi-reference lens-less Fourier-transform holography with a Greek-ladder sieve array. *Chin. Opt. Lett.* **2020**, *18*, 020901. [CrossRef]
107. Keskinbora, K.; Levitan, A.; Comin, R. Maskless Fourier transform holography. *Opt. Express* **2022**, *30*, 403–413. [CrossRef]
108. Cowley, J.M. 20 forms of electron holography. *Ultramicroscopy* **1992**, *41*, 335–348. [CrossRef]
109. Lichte, H.; Lehmann, M. Electron holography—Basics and applications. *Rep. Prog. Phys.* **2008**, *71*, 1–46. [CrossRef]
110. Harada, K.; Ono, Y.A.; Takahashi, Y. Lensless fourier transform electron holography applied to vortex beam analysis. *Microscopy* **2020**, *69*, 176–182. [CrossRef]
111. Harada, K.; Shimada, K.; Ono, Y.A. Electron holography for vortex beams. *Appl. Phys. Express* **2020**, *13*, 032003. [CrossRef]
112. Verbeeck, J.; Tian, H.; Schattschneider, P. Production and application of electron vortex beams. *Nature* **2010**, *467*, 301–304. [CrossRef]
113. Reuter, B.; Mahr, H. Experiments with Fourier-transform holograms using 4.48 nm X-rays. *J. Phys. E-Sci. Instrum.* **1976**, *9*, 746–751. [CrossRef]
114. Hellwig, O.; Eisebitt, S.; Eberhardt, W.; Schlotter, W.F.; Luning, J.; Stohr, J. Magnetic imaging with soft X-ray spectroholography. *J. Appl. Phys.* **2006**, *99*, 08h307. [CrossRef]
115. Scherz, A.; Schlotter, W.F.; Chen, K.; Rick, R.; Stohr, J.; Luning, J.; McNulty, I.; Gunther, C.; Radu, F.; Eberhardt, W.; et al. Phase imaging of magnetic nanostructures using resonant soft X-ray holography. *Phys. Rev. B* **2007**, *76*, 214410. [CrossRef]
116. Boutet, S.; Bogan, M.J.; Barty, A.; Frank, M.; Benner, W.H.; Marchesini, S.; Seibert, M.M.; Hajdu, J.; Chapman, H.N. Ultrafast soft X-ray scattering and reference-enhanced diffractive imaging of weakly scattering nanoparticles. *J. Electron Spectrosc.* **2008**, *166*, 65–73. [CrossRef]
117. Gunther, C.M.; Pfau, B.; Mitzner, R.; Siemer, B.; Roling, S.; Zacharias, H.; Kutz, O.; Rudolph, I.; Schondelmaier, D.; Treusch, R.; et al. Sequential femtosecond X-ray imaging. *Nature Photon.* **2011**, *5*, 99–102. [CrossRef]
118. Hellwig, O.; Gunther, C.M.; Radu, F.; Menzel, A.; Schlotter, W.F.; Luning, J.; Eisebitt, S. Ferrimagnetic stripe domain formation in antiferromagnetically-coupled Co/Pt-Co/Ni-Co/Pt multilayers studied via soft X-ray techniques. *Appl. Phys. Lett.* **2011**, *98*, 172503. [CrossRef]
119. Wang, T.H.; Zhu, D.L.; Wu, B.; Graves, C.; Schaffert, S.; Rander, T.; Muller, L.; Vodungbo, B.; Baumier, C.; Bernstein, D.P.; et al. Femtosecond single-shot imaging of nanoscale ferromagnetic order in Co/Pd multilayers using resonant X-ray holography. *Phys. Rev. Lett.* **2012**, *108*, 267403. [CrossRef]
120. Schaffert, S.; Pfau, B.; Geilhufe, J.; Gunther, C.M.; Schneider, M.; Schmising, C.V.; Eisebitt, S. High-resolution magnetic-domain imaging by Fourier transform holography at 21 nm wavelength. *New J. Phys.* **2013**, *15*, 093042. [CrossRef]
121. Geilhufe, J.; Pfau, B.; Schneider, M.; Buttner, F.; Gunther, C.M.; Werner, S.; Schaffert, S.; Guehrs, E.; Frommel, S.; Klaui, M.; et al. Monolithic focused reference beam X-ray holography. *Nat. Commun.* **2014**, *5*, 3008. [CrossRef]
122. Buettner, F.; Moutafis, C.; Schneider, M.; Krueger, B.; Guenther, C.M.; Geilhufe, J.; Schmising, C.V.; Mohanty, J.; Pfau, B.; Schaffert, S.; et al. Dynamics and inertia of skyrmionic spin structures. *Nat. Phys.* **2015**, *11*, 225–228. [CrossRef]
123. Pfau, B.; Gunther, C.M.; Hauet, T.; Eisebitt, S.; Hellwig, O. Thermally induced magnetic switching in bit-patterned media. *J. Appl. Phys.* **2017**, *122*, 043907. [CrossRef]
124. Geilhufe, J.; Pfau, B.; Gunther, C.M.; Schneider, M.; Eisebitt, S. Achieving diffraction -limited resolution in soft -X-ray Fourier -transform holography. *Ultramicroscopy* **2020**, *214*, 113005. [CrossRef] [PubMed]
125. Zayko, S.; Kfir, O.; Heigl, M.; Lohmann, M.; Sivis, M.; Albrecht, M.; Ropers, C. Ultrafast high-harmonic nanoscopy of magnetization dynamics. *Nat. Commun.* **2021**, *12*, 6337. [CrossRef] [PubMed]
126. Johnson, A.S.; Conesa, J.V.; Vidas, L.; Perez-Salinas, D.; Gunther, C.M.; Pfau, B.; Hallman, K.A.; Haglund, R.F.; Eisebitt, S.; Wall, S. Quantitative hyperspectral coherent diffractive imaging spectroscopy of a solid-state phase transition in vanadium dioxide. *Sci. Adv.* **2021**, *7*, eabf1386. [CrossRef] [PubMed]
127. Pratsch, C.; Rehbein, S.; Werner, S.; Guttmann, P.; Stiel, H.; Schneider, G. X-ray Fourier transform holography with beam shaping optical elements. *Opt. Express* **2022**, *30*, 15566–15574. [CrossRef]

128. Kern, L.M.; Pfau, B.; Schneider, M.; Gerlinger, K.; Deinhart, V.; Wittrock, S.; Sidiropoulos, T.; Engel, D.; Will, I.; Gunther, C.M.; et al. Tailoring optical excitation to control magnetic skyrmion nucleation. *Phys. Rev. B* **2022**, *106*, 054435. [CrossRef]
129. Suzuki, M.; Kondo, Y.; Isogami, S.; Tsunoda, M.; Takahashi, S.; Ishio, S. Hard X-Ray Fourier Transform Holography Using a Reference Scatterer Fabricated by Electron-Beam-Assisted Chemical-Vapor Deposition. In Proceedings of the 10th International Conference on X-ray Microscopy, Chicago, IL, USA, 15–20 August 2010; American Institute of Physics: Chicago, IL, USA, 2010; pp. 293–296.
130. Iwamoto, H.; Yagi, N. Hard X-ray Fourier transform holography from an array of oriented referenced objects. *J. Synchrotron Radiat.* **2011**, *18*, 564–568. [CrossRef]
131. Monserud, N.C.; Malm, E.B.; Wachulak, P.W.; Putkaradze, V.; Balakrishnan, G.; Chao, W.L.; Anderson, E.; Carlton, D.; Marconi, M.C. Recording oscillations of sub-micron size cantilevers by extreme ultraviolet Fourier transform holography. *Opt. Express* **2014**, *22*, 4161–4167. [CrossRef]
132. Thibault, P.; Esler, V. X-ray diffraction microscopy. *Annu. Rev. Condens. Matter Phys.* **2010**, *1*, 237–255. [CrossRef]
133. Chapman, H.N.; Nugent, K.A. Coherent lensless X-ray imaging. *Nat. Photon.* **2010**, *4*, 833–839. [CrossRef]
134. Nugent, K.A. Coherent methods in the X-ray sciences. *Adv. Phys.* **2010**, *59*, 1–99. [CrossRef]
135. Kaulich, B.; Thibault, P.; Gianoncelli, A.; Kiskinova, M. Transmission and emission X-ray microscopy: Operation modes, contrast mechanisms and applications. *J. Phys. Condes. Matt.* **2011**, *23*, 083002. [CrossRef]
136. Falcone, R.; Jacobsen, C.; Kirz, J.; Marchesini, S.; Shapiro, D.; Spence, J. New directions in X-ray microscopy. *Contemp. Phys.* **2011**, *52*, 293–318. [CrossRef]
137. Lider, V.V. X-ray holography. *Phys. Usp.* **2015**, *58*, 365–383. [CrossRef]
138. Bleiner, D. Tabletop beams for short wavelength spectrochemistry. *Spectroc. Acta Pt. B Atom. Spectr.* **2021**, *181*, 105978. [CrossRef]
139. Hauet, T.; Gunther, C.M.; Pfau, B.; Schabes, M.E.; Thiele, J.U.; Rick, R.L.; Fischer, P.; Eisebitt, S.; Hellwig, O. Direct observation of field and temperature induced domain replication in dipolar coupled perpendicular anisotropy films. *Phys. Rev. B* **2008**, *77*, 184421. [CrossRef]
140. Gunther, C.M.; Hellwig, O.; Menzel, A.; Pfau, B.; Radu, F.; Makarov, D.; Albrecht, M.; Goncharov, A.; Schrefl, T.; Schlotter, W.F.; et al. Microscopic reversal behavior of magnetically capped nanospheres. *Phys. Rev. B* **2010**, *81*, 064411. [CrossRef]
141. Latychevskaia, T.; Fink, H.-W. Practical algorithms for simulation and reconstruction of digital in-line holograms. *Appl. Opt.* **2015**, *54*, 2424–2434. [CrossRef]
142. Latychevskaia, T.; Fink, H.-W. Solution to the twin image problem in holography. *Phys. Rev. Lett.* **2007**, *98*, 233901. [CrossRef]
143. Latychevskaia, T. Iterative phase retrieval for digital holography. *J. Opt. Soc. Am. A* **2019**, *36*, D31–D40. [CrossRef]
144. Guehrs, E.; Fohler, M.; Frommel, S.; Gunther, C.M.; Hessing, P.; Schneider, M.; Shemilt, L.; Eisebitt, S. Mask-based dual-axes tomohholography using soft X-rays. *New J. Phys.* **2015**, *17*, 103042. [CrossRef]